

# Drone-Delivery Network for Opioid Overdose - Nonlinear Integer Queueing-Optimization Models and Methods

Miguel A. Lejeune <sup>\*</sup>, Wenbo Ma <sup>†</sup>

## Abstract

We propose a new stochastic emergency network design model that uses a fleet of drones to quickly deliver naxolone in response to opioid overdoses. The network is represented as a collection of  $M/G/K$  queueing systems in which the capacity  $K$  of each system is unknown ex-ante and modelled as a decision variable. The model is a bilocation-allocation optimization-based queueing problem which locates fixed (drone bases) and mobile (drones) servers and determines the drone dispatching decisions. The model takes the form of a nonlinear integer problem which is intractable in its original form. We provide a reformulation and algorithmic framework to allow for the exact solution of large instances. Our approach reformulates the multiple nonlinearities (fractional, polynomial, exponential, factorial terms) to give a mixed-integer linear programming (MILP) formulation. We demonstrate its generalizability and show that the problem of minimizing the average response time of a network of  $M/G/K$  queueing systems with unknown capacity  $K$  is always MILP-representable. We design two algorithms and demonstrate that the outer approximation branch-and-cut method is most efficient and scales well. The data-driven analysis based on real-life overdose data reveals that the use of drones could: 1) decrease the response time by 85%, 2) increase the survival chance by 466%, 3) save up to 36 additional lives per year, and 4) provide an additional quality-adjusted life year (QALY) of up to 305 years in Virginia Beach.

Key words: opioid overdose, drone delivery, optimization-based queueing model, survival chance, mixed-integer nonlinear programming, stochastic network design, outer approximation

## 1 Introduction

From 1999 to 2019, almost 500,000 people died from overdose in the USA [17] which is the leading cause of death for 25- to 64-year old US citizens. Opioid overdose is a life-threatening condition that, if not treated within minutes, can lead to severe neurological damage and death [13]. The chance of survival of an opiate overdose victim decreases by ten percent with each minute passing before resuscitation is attempted [14, 45]. Although emergency medical services (EMS) are located to optimize access to the population, the median arrival time of US EMS is between 7 and 8 minutes and can go beyond 14 minutes in rural, geographically challenged, or high-traffic urban areas [30]. In that respect, Gao et al. report that lessening the response time by one minute traditionally requires adding ambulances, each costing around \$200,000, whereas a \$10,000 drone can decrease the response time by two minutes. Consequently, medical drones are viewed as a promising way to reduce response times and to enhance EMS performance [48]. This motivates us to design a drone-based network to provide timely medical treatment and to study its potential to increase the chance of survival of overdose victims.

### 1.1 Background

The opioid overdose epidemic is ramping up as the number of incidents has quadrupled in the last 15 years. In the midst of this crisis, there are about 130 opioid overdose deaths each day [45]. The first

---

<sup>\*</sup>George Washington University, Washington, DC, USA; mlejeune@gwu.edu. M. Lejeune acknowledges the support of the National Science Foundation [Grant ECCS2114100] and [Grant ICER2022505]

<sup>†</sup>wenboma2011@gmail.com

wave of overdoses began in 1990s with an increase in the cases related to prescription opioids. The 2010 second wave was due to heroin while the third one, in 2013, was caused by synthetic opioids, in particular the illicitly manufactured Fentanyl [15]. The ongoing COVID-19 pandemic has further exacerbated the opioid health crisis [53]. According to the Centers for Disease Control and Prevention (CDC) [16], over 81,000 drug overdose deaths occurred in the USA between May 2019 and May 2020. Synthetic opioids are the primary driver behind the surge in overdose deaths. The death counts related to the synthetic opioid increased by 38.4% from the 12-month period ending in June 2019 to the 12-month period ending in May 2020. In addition to the substantial human toll, opioid overdose poses a great burden on the economy. The Society of Actuaries [54] estimated that the total economic cost of opioid misuse amounts to at least \$631 billions from 2015 to 2019 in the USA and includes the cost associated with healthcare services, premature mortality, criminal justice activity, and related educational and assistance program. As an illustration, the White House Council of Economic Advisers (CEA) estimated the 2015 total cost of opioid overdoses to \$504 billion, which includes \$431.7 billion due to mortality costs and \$72.3 billion due to health, productivity and criminal justice costs [12].

Many overdose-related deaths are preventable if naloxone, an overdose-reversal medication, can be administered within minutes following the breath cessation of the overdose victim [13]. Naloxone can be safely administered by a layperson witnessing an overdose incident [57] and its increased utilization has contributed to reducing the mortality rate of opioid overdoses as stressed in [36]. As opioids can slow or even entirely stop breathing, permanent brain damage can occur within only four minutes of oxygen deprivation. This underscores the need of administering naloxone timely to prevent brain damages or death and explains why naloxone access is of the US Department of Health and Human Services' three priority areas to combat the opioid crisis [31]. In order to mitigate the opioid crisis, Ornato et al. advocate the development of a system that allows 911 dispatchers, trained as drone pilots, to swiftly deliver naloxone with drones to bystanders and to guide them to administer naloxone.

Drones, also known as unmanned aerial vehicles (UAVs), are an emerging technology that can accomplish time-sensitive medical delivery tasks by fastening the time-to-scene response, particularly in the areas lacking established transportation network. A test in Detroit showed that the DJI 'Inspire 2' drones turned out to be systematically faster than ambulances – the traditional first responders – in delivering a naloxone nasal spray toolkit [55]. In order to make drone deliveries of naloxone strategy a reality and to leverage their full capability, drones need to be strategically deployed and assigned in a timely manner to the randomly arriving overdose-triggered requests (OTR) to account for the spatial and temporal uncertainty of opioid overdose incidents. The design of drone networks that sets up drone bases, prepositions drones, and determines their assignment to overdose emergencies remains an open problem in the literature. In that regard, Buckland et al. stress the need to develop drone network optimization models for opioid overdoses so that dispatchers "*understand when and where to dispatch drones*". This study is purported to fill this gap in the academic literature and the EMS practice.

## 1.2 Structure and Contributions

The contributions of this study are fourfold spanning across modeling, reformulation, algorithmic development, and emergency medical service practice.

**Modeling:** We develop a novel network design queueing-optimization model to help EMS operators respond quickly and efficiently to an opioid overdose via the drone-based delivery of naloxone. The proposed model is a stochastic service system design model with congestion [6] and determines the location of drone bases (DB) and drones as well as the assignment and dispatching of drones to overdose incidents. The model represents the drone network as a collection of  $M/G/K$  queueing systems in which the capacity  $K$  of each system (i.e., number drones at each opened DB) is unknown ex-ante and modelled as a decision variable. To our knowledge, there is no such model in the literature.

**Reformulation:** The base formulation of the proposed drone network design model is a NP-hard nonlinear integer problem which includes fractional, polynomial, exponential, and factorial terms. We derive in Theorem 4 a lifted mixed-integer linear programming (MILP) reformulation. Theorem 7 shows that the reformulation method is highly generalizable and that optimization models minimizing the average response time in networks organized as a series of interdependent  $M/G/K$  queueing systems with ex-ante unknown number of servers  $K$  are always MILP-representable.

**Algorithm:** We design two methods to solve the lifted MILP reformulation. The first one is an outer approximation algorithm based on the concept of lazy constraints to attenuate the challenges posed by the large dimension of the constraint space in the reformulation. The second and most efficient algorithm is an outer approximation branch-and-cut algorithm that involves the dynamic incorporation of valid inequalities and optimality-based cuts.

**Data-driven EMS insights:** Using real-life overdose data, we first demonstrate the extent to which the drone network contributes in reducing the response time, increasing the survival chance of overdose victims, and thereby in saving lives. A cross-validation analysis underlines the applicability and robustness of the network and its performance. Additional tests attest the low cost of implementing a drone network and its flexibility to adjust to the spatio-temporal uncertainty of overdose incidents. The quality-adjusted life year (QALY) underscores the largely increased quality of life and the related low incremental QALY cost. Second, we show the computational efficiency and scalability of the reformulation and algorithms.

The remainder of this paper is organized as follows. The literature review of the various fields intersecting with this study is in Section 2. Section 3 derives the closed-form formulas for the queueing metrics used to assess the performance of the drone response network, presents the base formulation of the proposed model, and analyzes its complexity. Section 4 is devoted to the reformulation method while Section 5 describes the proposed algorithms. Section 6 describes the data-driven study based on overdose real-life data from Virginia Beach, presents the computational efficiency of the method, and analyzes the healthcare benefits obtained by using drones to respond to overdose incidents. Section 7 provides concluding remarks.

## 2 Literature Review and Gaps

This study propose contributions spanning across three fields – drone-based response to opioid overdose, network design queueing models with mobile servers, and fractional 0-1 programming - which we review succinctly below.

### 2.1 Drone-based Response to Opioid Overdose

EMSs struggle to provide a timely response to medical emergencies leading to patients passing away due to the delayed arrival of ground ambulances [28, 43]. Medical drones are increasingly viewed as an efficient solution to assist EMS professionals, including for overdoses. They can quickly deliver medicine to patients and take on-sight imagery to support EMS personnel and operations before the arrival of ambulances [48]. We review next the scant literature on the use of drones for responding to overdoses.

Ye et al. propose a drone-delivery optimization model for overdoses. The model is solved with a genetic algorithm and is tested on suspected opioid overdose data from Durham County, NC. Their model reduces the response time to 4 minutes 38 seconds by using four drone bases (instead of 10 minutes 46 seconds with ambulances) that provide a 64.2% coverage of the county. Gao et al. propose an assignment Markov decision model to select which drone should be dispatch to a reported overdose incident and to relocate the drone afterwards. Confronted with the curse of dimensionality, the authors develop a state aggregation heuristic to derive a lookup table policy. A simulation based on EMS data from Indiana reveals that the state aggregation approach outperforms the myopic policy currently used in practice, in particular when the overall request intensity gets higher. The authors report the difficulty to properly estimate the value function used within their approach. In a pilot feasibility study based on 30 simulated opioid overdose events, Ornato et al. report that all participants were able to administer the intranasal naloxone medication to the manikin within about two minutes after the 911 contact and that 97% of them felt confident that they could do it successfully in a real event.

None of the above models consider jointly the location of the fixed (drone bases) and mobile (drones) servers and the assignment decisions. Additionally, these models are all covering models in which the objective is to minimize the total costs or the number of drones and/or stations. Our model contributes to fill in these two gaps in this literature. Our strategic network model 1) concurrently determines the location of the drone bases, the positioning of the drones, and the drone-dispatching policy to OTRs, and 2) is a survival network design model as it minimizes the response time which is the primary driver to increase the survival chance of overdosed patients.

### 2.2 Queueing-optimization Models for Stochastic Network Design

Queueing models can be categorized into two types: *descriptive* queueing models which conduct an after-the-fact analysis to analyze how a predefined system configuration has performed while *optimization-*

*based (prescriptive)* queuing models deal with congestion and are used for decision-making purposes (e.g., number of servers, location) [38]. We propose a new optimization-based queuing model that belongs to the class of stochastic network design queuing models with congestion [6]. This model class can be further decomposed into two sub-categories depending on whether the servers are fixed (immobile) requesting the customers to travel to the facility, or mobile and travel to the demand location. Since we consider the delivery of naloxone with drones, our literature review is focused on mobile servers, which is much less extensive than the one for immobile servers (see, e.g., [26]).

The first queuing optimization model with mobile server [8] determines the optimal location of a single facility in order to either maximize the service coverage or to minimize the response cost. Modelling the network as an M/G/1 system, the authors consider that, if the server is busy when the demand arrives, the demand can be either rejected (demand is lost and covered by backup servers at a cost) or enter a queue managed under the first-come-first-serve discipline. Building on this study, Chiu and Larson [20] consider a single facility operating as an M/G/k loss queuing system and show that, under a mild assumption, the optimal location reduces to a Hakimi median, which is the location minimizing the average travel time to a client [27]. Batt and Berman [4] study an M/G/k system that allows for queues with fixed number of servers  $K$  and develop an approximation-based approach to minimize the average response time. While the above studies consider a single facility, the queuing probabilistic location set-covering model proposed in [38] considers several facilities, each operating as an M/M/k queuing system. The authors determine the minimum number of facilities needed so that the probability of at least one server being available is greater than or equal to a certain threshold. Later, operating under the auspices of an M/G/k system, Marianov and ReVelle [37] study the probabilistic version of the maximal covering problem to show how to site a limited number of emergency vehicles with the objective of maximizing availability when a call arrives. Considering an M/M/k system, Aboolian et al. determine the optimal number of servers needed to minimize a cost function encompassing the setup cost to open facilities and operate servers, the travel costs, and the queuing delay costs. In the context of EMSs, Boutilier et al. propose a decoupled two-stage approach to set up the drone-based delivery of automated external defibrillators (AED) in Toronto. The first stage involves the heuristic solution of a set covering model to determine the number of DBs to open. In the second stage, each DB is assumed to operate as an M/M/k system and the objective, given the locations of the opened DBs set up in stage 1, is to minimize the number of drones needed to meet a specified response time goal. The expected service time of each drone and the arrival rates are fixed parameters determined ex-ante in an exogenous manner. An ongoing study [33] considers an M/G/1 queuing system for the delivery of AEDs to cardiac arrests and proposes new optimality-based bound tightening techniques.

In contrast to some of the above studies (see, e.g., [11]), this work considers that the service time and arrival rate of (overdose) requests assigned to drones are random variables whose parameters (mean) are endogenized. In addition to this, the proposed model considers that the capacity of the DBs is a

decision variable, which means, in other words, that the number of drones positioned at each DB is a decision variable. To our knowledge, this study is the first one that considers a system built as a collection of  $M/M/K_j$  servers in which the capacity or number of mobile servers  $K_j$  positioned at each facility is a bounded variable whose value can vary across the open DBs. We are not aware of any study that proposes a queuing-based optimization model to design a network of drones to deliver naloxone by locating and allocating drones in a stochastic environment that accounts for system congestion.

### 2.3 Fractional Nonlinear 0-1 Programming

As it will be shown in Section 3.3, the optimization problem studied is a nonlinear fractional integer problem in which the objective function is a ratio of two nonlinear functions each depending on integer variables. The class of problems closest to ours is that of fractional linear 0/1 (binary) problems for which significant improvements have been made over the last 5-6 years [10, 40]. Such problems pose serious computational challenges due to the pseudo-convexity and the combinatorial nature of the fractional objective. They minimize a single or a sum of ratios in which the denominator and numerator are both linear functions of binary variables. When more than one ratio term is in the objective functions, the problem (even unconstrained) has been shown to be NP-hard [46].

One approach to tackle fractional linear 0-1 programs is to move the fractional terms to the constraint set and to then derive MILP reformulations, which requires the introduction of continuous auxiliary variables and big-M constraints (see, e.g., [34]). MILP can however struggle – in particular when the number of ratio terms increases – due to the significant lifting of the decision and constraint spaces and the looseness of the continuous relaxation induced by the big-M constraints. Within this family, an MILP reformulation [10] based on the binary expansion of the integer-valued expressions appearing in the ratio terms permit to significantly lessen the number of bilinear terms and hence the number of linearization variables and constraints. This formulation scales much better but can also generate weak continuous relaxations, which hurts the convergence of the branch-and-bound algorithm. Mixed-integer second-order cone reformulations have also been proposed (e.g., [52]). They are based on the submodularity concept and the derivation of extended polymatroid cuts [2] to obtain tighter continuous relaxations. However, it is reported [40] that state-of-the-art optimization solvers still struggle to solve moderate-size mixed-integer conic problems and that their performance degrades quickly as size increases. Building upon the links between MILP and mixed-integer conic reformulations, Mehmanchi et al. derive tight convex continuous relaxations while limiting the lifting of the decision and constraint spaces.

The above methods, while providing very valuable insights, can not be directly used to the problem tackled here as the latter differs from the fractional 0-1 problem along several dimensions. First, the denominator and the numerator of each ratio term are nonconvex functions and each involve binary as well as general integer decision variables. Second, the objective function is the sum of a very large number (several hundred) of ratio terms. Third, the integer variables are multiplied by fractional

parameters which prohibits the use of the MILP method [10]. Fourth, the nonlinear terms are not simply bilinear. The numerator of each ratio term includes exponential terms and higher-degree polynomial terms while each denominator includes polynomial and factorial terms.

### 3 Drone Network Design Problem for Opioid Overdose Response

#### 3.1 Problem Description and Notations

The problem studied in this paper is called the Drone Network Design Problem for Opioid Overdose Response (DNDP). Consider an EMS provider that seeks to design a drone network to deliver naloxone, i.e., an opioid antagonist, to an opioid overdose incident with the objective to minimize the response time and thereby to maximize the chance of survival of the overdosed patient. Given a set of candidate locations (e.g., fire, police, EMS stations), some of them are selected to be set as drone bases where the available medical drones can be deployed. The DNDP model is a bilocation-allocation problem that simultaneously determines the locations of the DBs, the capacity of those (i.e., number of drones at each DB), and the response policy determined by the assignment of drones to OTRs in order to minimize the response time. The response time is defined as the sum of the queuing delay time experienced if drones are busy when requested for service and the drone flight time from a DB to an overdose location.

The following notational set is used in the formulation of the model (see Appendix A for the description of all notations). Let  $I$  be the set of opioid overdose locations and  $J$  be the set of potential DB locations. Let  $A_j$  be a vector of parameters  $(a_j, b_j, c_j)$  representing the coordinates of DB  $j$  in the earth-centered, earth-fixed coordinate system while  $A_i$  is a vector of parameters  $(a_i, b_i, c_i)$  representing the location  $i$  of an overdose. The parameter  $d_{ij} = \|A_i - A_j\|$  is the euclidean distance between DB  $j$  and overdose location  $i$ . A number  $p$  of drones with speed  $v$  can be deployed at up to  $q$  ( $q \leq p$ ) open DBs across the network. Due to battery and autonomy limitations, each drone has a limited coverage defined by its catchment area with radius  $r$ . A drone can only service OTRs at locations that are within its catchment radius [11, 19], since the drone must have enough power (i.e., battery coverage) to return to its base. Accordingly, we define the sets  $J_i, i \in I$  (resp.,  $I_j, j \in J$ ) which include all the DBs (resp., possible overdose locations) that are within  $r$  (i.e., the catchment area) of overdose location  $i$  (resp, DB  $j$ ). The binary decision variable  $x_j$  is equal to 1 if a DB is set up at location  $j$ , and is 0 otherwise. The binary variable  $y_{ij}$  takes value 1 if an OTR at  $i$  is assigned to DB  $j$ , and is equal to 0 otherwise. The general integer decision variable  $K_j$  represents the number of drones deployed at DB  $j$ . By convention, we denote the upper and lower bound of any decision variable  $x$  by  $\bar{x}$  and  $\underline{x}$ , respectively.

#### 3.2 DNDP Model: Collection of $M/G/K_j$ Queueing Systems with Unknown Capacity

The stochastic nature of the occurrence of overdoses and the resulting uncertainty about the arrival rates of OTRs at DBs along with the uncertain service times can cause delays, requests being queued, and

waiting times until a drone can be dispatched. In order to account for those, we model the network as a collection of  $M/G/K$  queues in which each DB  $j$  operates as an  $M/G/K_j$  queueing system where the capacity  $K_j$  of DB  $j$  is a bounded general integer decision variable representing the number of drones to be deployed at DB  $j$ . The occurrence of opioid overdoses at any location  $i$  follows a Poisson distribution with arrival rate  $\lambda_i$ . The service time of drones is a random variable with general distribution and with known first and second moments. The arrival rate  $\eta_j$  of OTRs at DB  $j$  can be inferred to be a Poisson process since it is a linear combination of independent Poisson variables (i.e., weighted sum of assigned OTRs; see (6)). The arrival rate of OTRs at DBs is unknown ex-ante and is defined endogenously via the solution of the optimization problem. The same applies to the drone service time whose expected value is also endogenized. It follows that the arrival process, i.e., demand at DBs and the service times of drones are endogenous sources of uncertainty with decision-dependent parameter (expected value) uncertainty as coined by [29]. If a drone cannot be dispatched on the spot after reception of an OTR, the request is placed in a queue depleted in a first-come-first-served manner. After providing service, drones travel back to the DB to be cleaned, recharged, and prepared for the next trip [45].

Having presented the structure of the network, we now derive closed-form functions for the queueing metrics - response time, queueing delay, and service time – needed to formulate the DNDP problem. We use the notations  $S_j$ ,  $R_i$ , and  $Q_j$  to represent the random variables respectively denoting the total service time at DB  $j$ , the response time for an overdose at location  $i$ , and the queueing delay at DB  $j$ .

Different from immobile servers, the travel time to and from the scene must be included in the service time for mobile servers [7]. The service time for any OTR at  $i$  serviced by a drone placed at DB  $j$  is [8]

$$S_{ij} = \frac{d_{ij}}{v} + \alpha_i + (\beta - 1)\frac{d_{ij}}{v} + \epsilon_i \quad (1)$$

where  $\beta$  is a constant that allows for different travel speeds to and from the scene, and  $\alpha_i$  and  $\epsilon_i$  are independent and identically distributed (i.i.d) random variables representing the on-scene service time and the drone's reset time (to be charged and prepared for the next demand), respectively. Let  $\xi_i = \alpha_i + \epsilon_i$  with expected value  $\mathbb{E}[\xi_i]$ . The expected value  $\mathbb{E}[S_{ij}]$  of the service time conditional to DB  $j$  responding to an OTR at  $i$  is:

$$\mathbb{E}[S_{ij}] = \beta \frac{d_{ij}}{v} + \mathbb{E}[\xi_i]. \quad (2)$$

The expected value of the total response time for  $j$  is the sum of the expected service times for all the OTRs serviced (i.e.,  $y_{ij} = 1$ ) by the drones stationed at  $j$  and depends on the dispatching variables  $y_{ij}$

$$\mathbb{E}[S_j] = \frac{\sum_{i \in I_j} \lambda_i y_{ij} \mathbb{E}[S_{ij}]}{\sum_{i \in I_j} \lambda_i y_{ij}} \quad (3)$$

while the second moment of the total service time at DB  $j$  is:

$$\mathbb{E}[S_j^2] = \frac{\sum_{i \in I_j} \lambda_i y_{ij} \mathbb{E}[S_{ij}^2]}{\sum_{i \in I_j} \lambda_i y_{ij}}. \quad (4)$$

The service time  $S_j$  follows a general unspecified distribution with known first and second moments and the opioid overdoses occur at each location  $i$  according to a Poisson process with rate  $\lambda_i$ . Accordingly, each DB  $j$  is modelled as an M/G/ $K_j$  queueing system in which a variable and upper bounded number  $K_j$  of drones can be stationed and whose expected queueing delay is given by [44, 50]

$$\mathbb{E}[Q_j] \approx \frac{\eta_j^{K_j} \mathbb{E}[S_j^2] \mathbb{E}[S_j]^{K_j-1}}{2(K_j-1)!(K_j - \eta_j \mathbb{E}[S_j])^2 \left[ \sum_{n=0}^{K_j-1} \frac{(\eta_j \mathbb{E}[S_j])^n}{n!} + \frac{(\eta_j \mathbb{E}[S_j])^{K_j}}{(K_j - \eta_j \mathbb{E}[S_j])} \right]} \quad (5)$$

which represents the expected waiting time until a drone is ready to be dispatched after reception of an OTR. The arrival rate of OTRs at DB  $j$  is given by

$$\eta_j = \sum_{i \in I_j} \lambda_i y_{ij}, \quad j \in J \quad (6)$$

which shows that the arrival rate is unknown ex-ante and depends on the assignment decisions  $y_{ij}$ , thereby highlighting the decision-dependent parameter uncertainty of the OTR arrivals at DBs.

The expected response time for an OTR at location  $i$  is:

$$\mathbb{E}[R_i] = \sum_{j \in J_i} \left( \mathbb{E}[Q_j] + \frac{d_{ij}}{v} \right) y_{ij}. \quad (7)$$

The metric used in the proposed optimization problem is the average (over all overdoses) of the response time. We denote it by  $\bar{R}$  and refer to it as the average response time.

**Theorem 1** *The functional form of the average response time is a fractional expression with nonlinear numerator and denominator:*

$$\bar{R} = \sum_{i \in I} \sum_{j \in J_i} \left[ \frac{\eta_j^{K_j} \mathbb{E}[S_j^2] \mathbb{E}[S_j]^{K_j-1}}{2(K_j-1)!(K_j - \eta_j \mathbb{E}[S_j])^2 \left[ \sum_{n=0}^{K_j-1} \frac{(\eta_j \mathbb{E}[S_j])^n}{n!} + \frac{(\eta_j \mathbb{E}[S_j])^{K_j}}{(K_j-1)(K_j - \eta_j \mathbb{E}[S_j])} \right]} + \frac{d_{ij}}{v} \right] \frac{\lambda_i y_{ij}}{\sum_{l \in I} \lambda_l} \quad (8)$$

**Proof:** The average response time is the weighted average of the expected response times for each OTR  $i$ . Therefore, we have:

$$\bar{R} = \sum_{i \in I} \frac{\lambda_i}{\sum_{l \in I} \lambda_l} \mathbb{E}[R_i] \quad (9)$$

Using the definition (7) of  $\mathbb{E}[R_i]$ , (9) becomes:

$$\bar{R} = \sum_{i \in I} \frac{\lambda_i}{\sum_{l \in I} \lambda_l} \sum_{j \in J_i} \left( \mathbb{E}[Q_j] + \frac{d_{ij}}{v} \right) y_{ij} = \sum_{i \in I} \sum_{j \in J_i} \left( \mathbb{E}[Q_j] + \frac{d_{ij}}{v} \right) \frac{\lambda_i y_{ij}}{\sum_{l \in I} \lambda_l} \quad (10)$$

Now expanding  $\mathbb{E}[Q_j]$  using (5), we obtain the expression given in Theorem 1.  $\square$

### 3.3 DNDP Base Model: Fractional Nonlinear Integer Programming Problem

We present now the base formulation of problem DNDP and analyze its complexity. The base formulation of DNDP belongs to the family of nonlinear fractional integer problems. Before presenting its formulation, we recall three of the most distinctive features of the proposed DNDP model. First, the minimization of the average response time is a survival objective function as it contributes to increasing the survival chance of the victims of opioid overdoses. Indeed, the probability of survival to an overdose is a monotone decreasing function of the response time. Second, the capacity – number of drones positioned at each DB – of each queuing system is not fixed ex-ante, but is a decision variable. Third, the queuing-optimization model accounts for the presence of congestion and decision-dependent uncertainty as some of the parameters characterizing the Poisson arrival process of OTRs at DBs and their service times are determined endogenously.

The fractional nonlinear integer base formulation **B – IFP** of problem DNDP is:

$$\mathbf{B - IFP} : \min \frac{1}{\sum_{l \in I} \lambda_l} \left[ \sum_{i \in I} \sum_{j \in J_i} \frac{\lambda_i d_{ij} y_{ij}}{v} + \sum_{i \in I} \sum_{j \in J_i} \frac{\lambda_i y_{ij} \sum_{l \in I_j} (\lambda_l y_{lj} \mathbb{E}[S_{lj}^2]) (\sum_{l \in I_j} \lambda_l y_{lj} \mathbb{E}[S_{lj}])^{K_j - 1}}{2(K_j - 1)! (K_j - \sum_{l \in I_j} \lambda_l y_{lj} \mathbb{E}[S_{lj}])^2 \left[ \sum_{n=0}^{K_j - 1} \frac{(\sum_{l \in I_j} \lambda_l y_{lj} \mathbb{E}[S_{lj}])^n}{n!} + \frac{(\sum_{l \in I_j} \lambda_l y_{lj} \mathbb{E}[S_{lj}])^{K_j}}{(K_j - 1)! (K_j - \sum_{l \in I_j} \lambda_l y_{lj} \mathbb{E}[S_{lj}])} \right]} \right] \quad (11a)$$

$$\text{s.to } \sum_{i \in I_j} \lambda_i y_{ij} \leq K_j \frac{\sum_{i \in I_j} \lambda_i y_{ij}}{\sum_{i \in I_j} \lambda_i y_{ij} \mathbb{E}[S_{ij}]}, \quad j \in J \quad (11b)$$

$$\sum_{j \in J_i} y_{ij} = 1, \quad i \in I \quad (11c)$$

$$y_{ij} \leq x_j \quad i \in I, j \in J_i \quad (11d)$$

$$\sum_{j \in J} x_j \leq q \quad (11e)$$

$$K_j \leq M x_j, \quad j \in J \quad (11f)$$

$$\sum_{j \in J} K_j = p \quad (11g)$$

$$x_j \in \{0, 1\}, \quad j \in J, \quad (11h)$$

$$y_{ij} \in \{0, 1\}, \quad i \in I, j \in J_i \quad (11i)$$

$$K_j \in \mathbb{Z}_+, \quad j \in J \quad (11j)$$

The objective function (11a) minimizes the average response time of the network, a key feature given the time-critical nature of opioid overdoses. Given that the queuing formulas used to represent the response time assume that the system is in steady-state, we introduce (11b) to ensure the steady-state condition and stability of the queuing system [39]. The nonlinear constraints (11b) prevent the arrival rate at any DB from exceeding its service rate. Constraint (11c) makes sure that each OTR is serviced by exactly one drone. Constraint (11d) requires that an OTR can only be assigned to an open DB within the

drone catchment area. Constraint (11e) limits from above the number of open DBs with the parameter  $q$ . Constraint (11f) ensures that drones can only be placed at an opened DB. The parameter  $M$  defines the maximum number (upper bound) of drones that can be stationed at any DB  $j$ :  $K_j \leq M, j \in J$ . As suggested in [41] and as implemented in [5, 25, 49] for medical drone networks, we set  $M$  equal to 2 as drones are scarce resources and are typically spread in order to expand the coverage of the network. Constraint (11g) ensures that all available drones are deployed. The binary and general integer nature of the decision variables are respectively enforced by (11h), (11i), and (11j) with  $\mathbb{Z}_+$  denoting the set of nonnegative integer numbers.

Proposition 2 follows immediately from the above discussion.

**Proposition 2** *Problem B – IFP is an NP-hard optimization problem in which:*

- (i) *The objective function is neither convex, nor concave: the denominator and the numerator in each ratio term of the objective function are nonlinear and nonconvex functions.*
- (ii) *The ratio terms can involve division by 0 and be indeterminate.*
- (iii) *The ratio term corresponding to a location where no DB is set up is undefined.*
- (iv) *There is a mix of binary and bounded general integer variables.*
- (v) *The nonlinear constraints (11b) include fractional and polynomial terms, can be indeterminate, and define a nonconvex feasible area.*
- (vi) *The continuous relaxation of B – IFP is a nonconvex programming problem.*

**Proof:** It has been shown [46] that the unconstrained 0-1 linear- fractional problem is NP-hard when the objective function sums two or more ratio terms. The NP-hardness of **B – IFP** follows immediately since it adds additional complexity sources (constraints, nonlinear denominator and numerator in ratios, etc.).

- (i) The numerator and denominator include polynomial and exponential terms. The denominator has also factorial and fractional terms. Both are nonconvex functions. It can be easily shown that the hessian matrix of the fractional objective function is not positive semidefinite, nor negative semidefinite.
- (ii) Any term  $(K_j - \sum_{l \in I_j} \lambda_l y_{lj} \mathbb{E}[S_{lj}])$  can be equal to 0, which leads to a division by 0, if 1) the service rate is equal to the arrival rate at a DB  $j$  or 2) if no DB is set up at location  $j$ , thereby implying  $K_j = y_{ij} = 0, \forall i \in J_j$ .
- (iii) If no DB is set up at the potential location  $j$ , no drone can be stationed at  $j$ , which implies that  $K_j = 0$ . In that case, the denominator includes a term involving taking the factorial of a negative number:  $(K_j - 1)! = (-1)!$
- (iv) Obvious: see constraints (11h)-(11j).
- (v) The right-hand side is fractional with a bilinear numerator and linear denominator.
- (vi) See part (i).

We propose in Appendix B an illustration for a small network and present the formulation of the objective function in **B – IFP**.

## 4 Reformulation Framework

Proposition 2 highlights that the base formulation **B – IFP** is an NP-hard fractional nonlinear integer problem and is extremely difficult to solve numerically even for problem instances of small size. We propose in this section an equivalent and computationally tractable reformulation of the problem that takes the form of a mixed-integer linear programming (MILP) problem. We first demonstrate (Theorem 4) that an MILP reformulation can be derived when the number of servers is two or less as relevant to the considered medical drone network problem (see [5, 41, 49]) before generalizing this result (Theorem 7) to any  $M/G/K$  queueing system with variable number of servers  $K_j$  at each facility  $j$ .

The derivation of the reformulation is relatively complex and we split it two main steps – presented in Proposition 3 and Theorem 4 – to ease the exposition. Proposition 3 proposes an equivalent reformulation taking the form of a fractional nonlinear binary problem **R-BFP** with nonconvex continuous relaxation.

**Proposition 3** *Let  $\gamma_j^m \in \{0, 1\}$ ,  $j \in J, m = 1, \dots, M$ . The fractional nonlinear binary problem*

$$\begin{aligned} \mathbf{R - BFP} : \min & \sum_{i \in I} \sum_{j \in J_i} \frac{y_{ij} d_{ij} \lambda_i}{v \sum_{l \in I} \lambda_l} + \sum_{i \in I} \sum_{j \in J_i} \sum_{m=1}^M \frac{y_{ij} \lambda_i}{\sum_{l \in I} \lambda_l} & (12a) \\ & \left[ \frac{\gamma_j^m \sum_{l \in I_j} \lambda_l y_{lj} \mathbb{E}[S_{lj}^2] (\sum_{l \in I_j} \lambda_l y_{lj} \mathbb{E}[S_{lj}])^{m-1}}{2(m-1)!(m - \sum_{l \in I_j} \lambda_l y_{lj} \mathbb{E}[S_{lj}])^2 \left[ \sum_{n=0}^{m-1} \frac{(\sum_{l \in I_j} \lambda_l y_{lj} \mathbb{E}[S_{lj}])^n}{n!} + \frac{(\sum_{l \in I_j} \lambda_l y_{lj} \mathbb{E}[S_{lj}])^m}{(m-1)!(m - \sum_{l \in I_j} \lambda_l y_{lj} \mathbb{E}[S_{lj}])} \right]} \right] \\ & \text{s.to (11c) – (11e); (11h) – (11i)} \end{aligned}$$

$$\sum_{i \in I_j} \lambda_i y_{ij} \mathbb{E}[S_{ij}] \leq \sum_{m=1}^M m \gamma_j^m, \quad j \in J \quad (12b)$$

$$\sum_{m=1}^M m \gamma_j^m \leq M x_j, \quad j \in J \quad (12c)$$

$$\sum_{j \in J} \sum_{m=1}^M m \gamma_j^m = p \quad (12d)$$

$$\sum_{m=1}^M \gamma_j^m \leq 1, \quad j \in J \quad (12e)$$

$$\gamma_j^m \in \{0, 1\}, \quad j \in J, m = 1, \dots, M \quad (12f)$$

is equivalent to the fractional nonlinear integer problem **B – IFP**.

**Proof:** Part (i): We first replace each bounded general integer variable  $K_j$  by a weighted sum of  $M$  binary variables  $\gamma_j^m, m = 1, \dots, M$  in the set of constraints. For this variable substitution to work, the following relationship must be enforced:

$$K_j := \sum_{m=1}^M m \gamma_j^m. \quad (13)$$

This is accomplished in two steps. First, we introduce the linear constraints

$$\sum_{m=1}^M \gamma_j^m \leq 1 \quad (14a)$$

$$\gamma_j^m \in \{0, 1\} \quad m = 1, \dots, M \quad (14b)$$

for each  $j \in J$  (see (12e) and (12f)) to ensure that  $\sum_{m=1}^M m\gamma_j^m$  can take any integer value in  $\{0, M\}$  which is the restriction imposed on each  $K_j$  via (11f) and (11j). Accordingly, we substitute (12e)-(12f) for (11j) and then replace  $K_j$  by the right-side term of (13) in (11b), (11f), and (11g). The constraints (11b), (11f), and (11g) can then be replaced by (12b), (12c), and (12d) in the constraint set of **R – BFP**. Additionally, we also need to divide both sides of (11b) by  $\sum_{i \in I_j} \lambda_i y_{ij}$  to obtain its linear equivalent (12b). This gives the mixed-integer feasible set given in the statement of Proposition 3.

Part (ii): We now remove the general integer variables  $K_j$  from the objective function. In each ratio term

$$\frac{\sum_{l \in I_j} \lambda_l y_{lj} \mathbb{E}[S_{lj}^2] (\sum_{l \in I_j} \lambda_l y_{lj} \mathbb{E}[S_{lj}])^{K_j-1}}{2(K_j - 1)! (K_j - \sum_{l \in I_j} \lambda_l y_{lj} \mathbb{E}[S_{lj}])^2 \left[ \sum_{n=0}^{K_j-1} \frac{(\sum_{l \in I_j} \lambda_l y_{lj} \mathbb{E}[S_{lj}])^n}{n!} + \frac{(\sum_{l \in I_j} \lambda_l y_{lj} \mathbb{E}[S_{lj}])^{K_j}}{(K_j-1)! (K_j - \sum_{l \in I_j} \lambda_l y_{lj} \mathbb{E}[S_{lj}])} \right]} \quad (15)$$

of the objective function, we first replace the general integer decision variable  $K_j$  by the index parameter  $m$ , which gives:

$$\frac{\sum_{l \in I_j} \lambda_l y_{lj} \mathbb{E}[S_{lj}^2] (\sum_{l \in I_j} \lambda_l y_{lj} \mathbb{E}[S_{lj}])^{m-1}}{2(m-1)! (m - \sum_{l \in I_j} \lambda_l y_{lj} \mathbb{E}[S_{lj}])^2 \left[ \sum_{n=0}^{m-1} \frac{(\sum_{l \in I_j} \lambda_l y_{lj} \mathbb{E}[S_{lj}])^n}{n!} + \frac{(\sum_{l \in I_j} \lambda_l y_{lj} \mathbb{E}[S_{lj}])^m}{(m-1)! (m - \sum_{l \in I_j} \lambda_l y_{lj} \mathbb{E}[S_{lj}])} \right]} \quad (16)$$

Next, we multiply each expression (16) by the corresponding binary variable  $\gamma_j^m$

$$\frac{\gamma_j^m \sum_{l \in I_j} \lambda_l y_{lj} \mathbb{E}[S_{lj}^2] (\sum_{l \in I_j} \lambda_l y_{lj} \mathbb{E}[S_{lj}])^{m-1}}{2(m-1)! (m - \sum_{l \in I_j} \lambda_l y_{lj} \mathbb{E}[S_{lj}])^2 \left[ \sum_{n=0}^{m-1} \frac{(\sum_{l \in I_j} \lambda_l y_{lj} \mathbb{E}[S_{lj}])^n}{n!} + \frac{(\sum_{l \in I_j} \lambda_l y_{lj} \mathbb{E}[S_{lj}])^m}{(m-1)! (m - \sum_{l \in I_j} \lambda_l y_{lj} \mathbb{E}[S_{lj}])} \right]} \quad (17)$$

and sum the resulting ratio terms (17) over  $m$  ( $m = 1, \dots, M$ ) which represents the possible number of drones positioned at any open DB

$$\sum_{m=1}^M \frac{\gamma_j^m \sum_{l \in I_j} \lambda_l y_{lj} \mathbb{E}[S_{lj}^2] (\sum_{l \in I_j} \lambda_l y_{lj} \mathbb{E}[S_{lj}])^{m-1}}{2(m-1)! (m - \sum_{l \in I_j} \lambda_l y_{lj} \mathbb{E}[S_{lj}])^2 \left[ \sum_{n=0}^{m-1} \frac{(\sum_{l \in I_j} \lambda_l y_{lj} \mathbb{E}[S_{lj}])^n}{n!} + \frac{(\sum_{l \in I_j} \lambda_l y_{lj} \mathbb{E}[S_{lj}])^m}{(m-1)! (m - \sum_{l \in I_j} \lambda_l y_{lj} \mathbb{E}[S_{lj}])} \right]} \quad (18)$$

Due to (12e), at most one of the binary variables  $\gamma_j^m$  for each  $j \in J$  takes a non-zero value (i.e., 1) and, therefore, at most one of the terms in the summation is (18) is non-zero. This, combined with the fact that the feasible set of **R – BFP** ensures that (13) holds true for each  $j$  (see Part i)), shows that (18) is equivalent to (15).

Two cases are now to be considered. First, if for any arbitrary  $j \in J$ , we have  $K_j = 0$ , then each  $\gamma_j^m, m = 1, \dots, M$  is equal to 0 since the constraints in **R – BFP** imply (13), and the expression in (18) is

equal to 0. Second, if  $K_j \neq 0$  with  $K_j \leq M$ , then exactly one of the  $\gamma_j^m, m = 1, \dots, M$  is equal to 1. More precisely, due to (13), we have  $\gamma_j^{K_j} = 1$  and  $\gamma_j^m = 0, m = 1, \dots, M, m \neq K_j$ . This means that the only term in (18) taking a non-zero value is the one for which  $m = K_j$ , which in turn implies that (18) is equal to (15), and provides the result that we set out to prove.  $\square$

The following comments are worth noting. A first difference with **B – IFP** is that **R – BFP** has only binary decision variables and does not include any general integer variables  $K_j$ . The second difference and advantage of **R – BFP** over **I – BFP** is that the polynomial terms in the reformulation **R – BFP** are of lower degree than those in **B – IFP**. Third, in **R – BFP**, there is no decision variable  $K_j$  appearing in the upper limits of the summation operations, such as  $\sum_{n=0}^{K_j-1} (\sum_{l \in I_j} \lambda_l y_{lj}) \mathbb{E}[S_{lj}] y^n$  in **B – IFP**. Fourth, there is no exponential term of form  $y_{ij}^{K_j}$  in **R – BFP**. Fifth, the factorial terms  $(K_j - 1)!$  in **B – IFP** which, besides being nonlinear, can also be undefined if  $K_j = 0$ , are no longer present in **R – BFP** in which they are replaced by the fixed parameters  $(m - 1)!$ . The undefined issue is resolved since  $m$  is at least equal to 1. The reformulation **R – BFP** is valid for any value assigned to  $M$ .

The constraints (11c)-(11e), (11h)-(11i), and (12b)-(12f) representing the feasible area of problem **R-BFP** define collectively a linear binary feasible set which, to ease the notation, will be thereafter referred to with the notation  $\mathcal{BL}$ :

$$\mathcal{BL} = \left\{ (x, y, \gamma) \in \{0, 1\}^{|J| + \sum_{i \in I} |J_i| + M|J|} : (11c) - (11e); (11h) - (11i); (12b) - (12f) \right\}. \quad (19)$$

We derive in Appendix B the objective function of problem **R – BFP** for a small network. Table 8 in Appendix C specifies the number of constraints and integer decision variables of each type in the base formulation **B – IFP** and its reformulation **R – BFP**.

Although simpler than **B – IFP**, **R – BFP** is still a challenging optimization problem as it involves polynomial and fractional terms and its continuous relaxation is nonconvex. We shall now demonstrate in Theorem 4 that the MILP problem **R – MILP** is equivalent to **R – BFP** and **B – IFP**. The proof is split into two main steps that starts with the moving of the fractional terms from the objective function into the constraint set and continues with the linearization of the polynomial terms. To shorten the notations in the proof, we replace  $\mathbf{E}[S_{lj}]$  and  $\mathbf{E}[S_{lj}^2]$  by  $\tilde{S}_{lj}$  and  $\tilde{S}_{lj}^2$ , respectively. We first consider the medical drone network design problem DNDP in which  $M = 2$  (i.e., up to two servers per DB). Theorem 7 will later demonstrate that an MILP reformulation can be derived for any value of the parameter  $M$ , or, in other words, for any M/G/K queuing system in which the capacity of each queuing system (i.e., number of servers) is unknown and variable.

**Theorem 4** *Define the index sets  $D_j = \{(l, t) : l, t \in I_j, l < t\}, j \in J$ . Let  $z_{lt}^j \in [0, 1], \mu_{ij}^m \in [0, \bar{U}_j^m], \tau_{lt}^j \in [0, \bar{U}_j^2]$ , and  $\omega_{ij}^m \in [0, \bar{\mu}_{ij}^m], i, l, t \in I_j, (l, t) \in D_j, j \in J, m = 1, \dots, M$  be continuous auxiliary variables defined by the linearization sets:*

$$\mathcal{M}_{z_{lt}^j} := \left\{ (y, z) \in \{0, 1\}^2 \times [0, 1] : \begin{array}{l} z_{lt}^j \geq 0 \\ z_{lt}^j \geq y_{tj} + y_{lj} - 1 \\ z_{lt}^j \leq y_{tj} \\ z_{lt}^j \leq y_{lj} \end{array} \right\} \quad \begin{array}{l} (20a) \\ (20b) \\ (20c) \\ (20d) \end{array}$$

$$\mathcal{M}_{\mu_{lj}^m} := \left\{ (y, U, \mu) \in \{0, 1\} \times R_+^2 : \begin{array}{l} \mu_{lj}^m \geq \underline{U}_j^m y_{lj} \\ \mu_{lj}^m \geq \overline{U}_j^m (y_{lj} - 1) + U_j^m \\ \mu_{lj}^m \leq \overline{U}_j^m y_{lj} \\ \mu_{lj}^m \leq \underline{U}_j^m (y_{lj} - 1) + U_j^m \end{array} \right\} \quad \begin{array}{l} (21a) \\ (21b) \\ (21c) \\ (21d) \end{array}$$

$$\mathcal{M}_{\tau_{lt}^j} := \left\{ (z, U, \tau) \in \{0, 1\} \times R_+^2 : \begin{array}{l} \tau_{lt}^j \geq \underline{U}_j^2 z_{lt}^j \\ \tau_{lt}^j \geq \overline{U}_j^2 (z_{lt}^j - 1) + U_j^2 \\ \tau_{lt}^j \leq \overline{U}_j^2 z_{lt}^j \\ \tau_{lt}^j \leq \underline{U}_j^2 (z_{lt}^j - 1) + U_j^2 \end{array} \right\} \quad \begin{array}{l} (22a) \\ (22b) \\ (22c) \\ (22d) \end{array}$$

$$\mathcal{M}_{\omega_{ij}^m} := \left\{ (\gamma, \mu, \omega) \in \{0, 1\} \times R_+^2 : \begin{array}{l} \omega_{ij}^m \geq \underline{\mu}_{ij}^m \gamma_j^m \\ \omega_{ij}^m \geq \overline{\mu}_{ij}^m (\gamma_j^1 - 1) + \mu_{ij}^m \\ \omega_{ij}^m \leq \overline{\mu}_{ij}^m \gamma_j^m \\ \omega_{ij}^m \leq \underline{\mu}_{ij}^m (\gamma_j^1 - 1) + \mu_{ij}^m \end{array} \right\} \quad \begin{array}{l} (23a) \\ (23b) \\ (23c) \\ (23d) \end{array}$$

The MILP problem **R – MILP**

$$\min \sum_{i \in I} \sum_{j \in J_i} \frac{y_{ij} d_{ij} \lambda_i}{v \sum_{l \in I} \lambda_l} + \sum_{i \in I} \sum_{j \in J_i} \left[ \frac{\omega_{ij}^1}{2} + \frac{\omega_{ij}^2}{2} \right] \frac{\lambda_i}{\sum_{l \in I} \lambda_l} \quad (24a)$$

s.to  $(x, y, \gamma) \in \mathcal{BL}$

$$U_j^1 = \sum_{l \in I_j} \lambda_l \mu_{lj}^1 \tilde{S}_{lj} + \sum_{l \in I_j} \lambda_l y_{lj} \tilde{S}_{lj}^2 \quad j \in J \quad (24b)$$

$$4U_j^2 = \sum_{l \in I_j} (\lambda_l)^2 \tilde{S}_{lj}^2 (\mu_{lj}^2 + y_{lj} \tilde{S}_{lj}) + 2 \sum_{l, t \in D_j} \lambda_l \lambda_t \tilde{S}_{lj} (z_{lt}^j \tilde{S}_{lj}^2 + \tilde{S}_{lt} \tau_{lt}^j) \quad j \in J \quad (24c)$$

$$(y, z) \in \mathcal{M}_{z_{lt}^j} \quad (l, t) \in D_j, j \in J$$

$$(y, U, \mu) \in \mathcal{M}_{\mu_{lj}^r} \quad l \in I_j, j \in J, r = 1, \dots, M$$

$$(z, U, \tau) \in \mathcal{M}_{\tau_{lt}^j} \quad (l, t) \in D_j, j \in J$$

$$(\gamma, \mu, \omega) \in \mathcal{M}_{\omega_{ij}^r} \quad i \in I, j \in J_i, r = 1, \dots, M$$

is equivalent to the nonlinear integer problems **B – IFP** and **R – BFP** for  $M=2$ .

**Proof:** For  $M = 2$ , the fractional terms

$$\sum_{m=1}^M \left[ \frac{\gamma_j^m \sum_{l \in I_j} \lambda_l y_{lj} \tilde{S}_{lj}^2 (\sum_{l \in I_j} \lambda_l y_{lj} \tilde{S}_{lj})^{m-1}}{2(m-1)!(m - \sum_{l \in I_j} \lambda_l y_{lj} \tilde{S}_{lj})^2 \left[ \sum_{n=0}^{m-1} \frac{(\sum_{l \in I_j} \lambda_l y_{lj} \tilde{S}_{lj})^n}{n!} + \frac{(\sum_{l \in I_j} \lambda_l y_{lj} \tilde{S}_{lj})^m}{(m-1)!(m - \sum_{l \in I_j} \lambda_l y_{lj} \tilde{S}_{lj})} \right]} \right] \quad (25)$$

in (12a) can be rewritten as

$$\frac{1}{2} \left[ \frac{\gamma_j^1 \sum_{l \in I_j} \lambda_l y_{lj} \tilde{S}_{lj}^2}{(1 - \sum_{l \in I_j} \lambda_l y_{lj} \tilde{S}_{lj})} + \frac{\gamma_j^2 \sum_{l \in I_j} \lambda_l y_{lj} \tilde{S}_{lj}^2 \sum_{l \in I_j} \lambda_l y_{lj} \tilde{S}_{lj}}{(2 - \sum_{l \in I_j} \lambda_l y_{lj} \tilde{S}_{lj})^2 + (2 - \sum_{l \in I_j} \lambda_l y_{lj} \tilde{S}_{lj})^2 \sum_{l \in I_j} \lambda_l y_{lj} \tilde{S}_{lj} + (2 - \sum_{l \in I_j} \lambda_l y_{lj} \tilde{S}_{lj})(\sum_{l \in I_j} \lambda_l y_{lj} \tilde{S}_{lj})^2} \right]$$

In order to remove the fractional terms from the objective function, we introduce the nonnegative auxiliary variables  $U_j^m$ ,  $m = 1, 2$  defined as:

$$U_j^1 = \frac{\sum_{l \in I_j} \lambda_l y_{lj} \tilde{S}_{lj}^2}{1 - \sum_{l \in I_j} \lambda_l y_{lj} \tilde{S}_{lj}} \quad (26)$$

$$U_j^2 = \frac{\sum_{l \in I_j} \lambda_l y_{lj} \tilde{S}_{lj}^2 \sum_{l \in I_j} \lambda_l y_{lj} \tilde{S}_{lj}}{(2 - \sum_{l \in I_j} \lambda_l y_{lj} \tilde{S}_{lj})^2 + (2 - \sum_{l \in I_j} \lambda_l y_{lj} \tilde{S}_{lj})^2 \sum_{l \in I_j} \lambda_l y_{lj} \tilde{S}_{lj} + (2 - \sum_{l \in I_j} \lambda_l y_{lj} \tilde{S}_{lj})(\sum_{l \in I_j} \lambda_l y_{lj} \tilde{S}_{lj})^2} \quad (27)$$

Problem **R-BFP** can now be equivalently rewritten as:

$$\begin{aligned} \min \quad & \sum_{i \in I} \sum_{j \in J} \frac{y_{ij} d_{ij} \lambda_i}{v \sum_{l \in I} \lambda_l} + \sum_{i \in I} \sum_{j \in J} \left[ \frac{\gamma_j^1 y_{ij} U_j^1}{2} + \frac{\gamma_j^2 y_{ij} U_j^2}{2} \right] \frac{\lambda_i}{\sum_{l \in I} \lambda_l} \\ \text{s.to} \quad & (26) - (27) \\ & (x, y, \gamma) \in \mathcal{BL} \end{aligned} \quad (28)$$

The second step is the linearization of the nonconvex equality constraints (26) and (27) and the polynomial terms of the objective function (28). Multiplying both sides of (26) by  $(1 - \sum_{l \in I_j} \lambda_l y_{lj} \tilde{S}_{lj})$  gives

$$U_j^1 = \sum_{l \in I_j} \lambda_l y_{lj} U_j^1 \tilde{S}_{lj} + \sum_{l \in I_j} \lambda_l y_{lj} \tilde{S}_{lj}^2, \quad j \in J \quad (29)$$

which can be linearized as (24b) by introducing the linearization auxiliary variables  $\mu_{lj}^1$  and the McCormick inequalities (21a)-(21d) in the set  $\mathcal{M}_{\mu_{lj}^1}$  to ensure that:  $\mu_{lj}^1 = y_{lj} U_j^1$ ,  $l \in I_j$ ,  $j \in J$ .

Similarly, multiplying both sides of (27) by

$$(2 - \sum_{l \in I_j} \lambda_l y_{lj} \tilde{S}_{lj})^2 + (2 - \sum_{l \in I_j} \lambda_l y_{lj} \tilde{S}_{lj})^2 \sum_{l \in I_j} \lambda_l y_{lj} \tilde{S}_{lj} + (2 - \sum_{l \in I_j} \lambda_l y_{lj} \tilde{S}_{lj})(\sum_{l \in I_j} \lambda_l y_{lj} \tilde{S}_{lj})^2$$

gives

$$\begin{aligned} & U_j^2 \left( (2 - \sum_{l \in I_j} \lambda_l y_{lj} \tilde{S}_{lj})^2 + (2 - \sum_{l \in I_j} \lambda_l y_{lj} \tilde{S}_{lj})^2 \sum_{l \in I_j} \lambda_l y_{lj} \tilde{S}_{lj} + (2 - \sum_{l \in I_j} \lambda_l y_{lj} \tilde{S}_{lj})(\sum_{l \in I_j} \lambda_l y_{lj} \tilde{S}_{lj})^2 \right) \\ & = \sum_{l \in I_j} \lambda_l y_{lj} (\tilde{S}_{lj})^2 \sum_{l \in I_j} \lambda_l y_{lj} \tilde{S}_{lj} \end{aligned} \quad (30)$$

The left-hand side of (30) can be rewritten as

$$\begin{aligned}
& U_j^2 \left( 2 - \sum_{l \in I_j} \lambda_l y_{lj} \tilde{S}_{lj} \right) \times \left[ 2 - \sum_{l \in I_j} \lambda_l y_{lj} \tilde{S}_{lj} + (2 - \sum_{l \in I_j} \lambda_l y_{lj} \tilde{S}_{lj}) \sum_{l \in I_j} \lambda_l y_{lj} \tilde{S}_{lj} + \left( \sum_{l \in I_j} \lambda_l y_{lj} \tilde{S}_{lj} \right)^2 \right] \\
&= U_j^2 \left( 2 - \sum_{l \in I_j} \lambda_l y_{lj} \tilde{S}_{lj} \right) \times \left[ 2 - \sum_{l \in I_j} \lambda_l y_{lj} \tilde{S}_{lj} + 2 \sum_{l \in I_j} \lambda_l y_{lj} \tilde{S}_{lj} - \left( \sum_{l \in I_j} \lambda_l y_{lj} \tilde{S}_{lj} \right)^2 + \left( \sum_{l \in I_j} \lambda_l y_{lj} \tilde{S}_{lj} \right)^2 \right] \\
&= U_j^2 \left( 2 - \sum_{l \in I_j} \lambda_l y_{lj} \tilde{S}_{lj} \right) \left( 2 + \sum_{l \in I_j} \lambda_l y_{lj} \tilde{S}_{lj} \right) = U_j^2 \left( 4 - \sum_{l \in I_j} \lambda_l y_{lj} \tilde{S}_{lj} \sum_{l \in I_j} \lambda_l y_{lj} \tilde{S}_{lj} \right) \\
&= U_j^2 \left( 4 - \sum_{l \in I_j} \sum_{t \in I_j} \lambda_l \lambda_t y_{lj} y_{tj} \tilde{S}_{lj} \tilde{S}_{tj} \right). \tag{31a}
\end{aligned}$$

The double summation expression in (31a) can be simplified. First, using the idempotent identity of binary variables, we have:  $(y_{lj})^2 = y_{lj}$ . Second, we split the summands in (31a) into two parts including respectively the separable bilinear terms  $(y_{lj})^2$  and the nonseparable ones  $y_{lj}y_{tj}$ ,  $l \neq t$ :

$$\sum_{l \in I_j} \sum_{t \in I_j} \lambda_l \lambda_t y_{lj} y_{tj} \tilde{S}_{lj} \tilde{S}_{tj} = \sum_{l \in I_j} (\lambda_l)^2 y_{lj} (\tilde{S}_{lj})^2 + 2 \sum_{(l,t) \in D_j} \lambda_l \lambda_t y_{lj} y_{tj} \tilde{S}_{lj} \tilde{S}_{tj}. \tag{32}$$

Combining (31) and (32), we reformulate the left side of (30) as:

$$U_j^2 \left( 4 - \sum_{l \in I_j} (\lambda_l)^2 y_{lj} (\tilde{S}_{lj})^2 - 2 \sum_{(l,t) \in D_j} \lambda_l \lambda_t y_{lj} y_{tj} \tilde{S}_{lj} \tilde{S}_{tj} \right) \tag{33}$$

Using the same reasoning, the right-hand side of (30) is equal to

$$\sum_{l \in I_j} (\lambda_l)^2 y_{lj} (\tilde{S}_{lj})^2 \tilde{S}_{lj} + 2 \sum_{(l,t) \in D_j} \lambda_l \lambda_t y_{lj} y_{tj} (\tilde{S}_{lj})^2 \tilde{S}_{tj}.$$

Thus, (27) and (30) are equivalent to

$$\begin{aligned}
& U_j^2 \left( 4 - \sum_{l \in I_j} (\lambda_l)^2 y_{lj} (\tilde{S}_{lj})^2 - 2 \sum_{(l,t) \in D_j} \lambda_l \lambda_t y_{lj} y_{tj} \tilde{S}_{lj} \tilde{S}_{tj} \right) \\
&= \sum_{l \in I_j} (\lambda_l)^2 y_{lj} (\tilde{S}_{lj})^2 \tilde{S}_{lj} + 2 \sum_{(l,t) \in D_j} \lambda_l \lambda_t y_{lj} y_{tj} (\tilde{S}_{lj})^2 \tilde{S}_{tj}, \tag{34}
\end{aligned}$$

which defines a nonlinear equality constraint including bilinear terms  $U_j^2 y_{lj}$ ,  $y_{lj} y_{tj}$  and trilinear terms  $U_j^2 y_{lj} y_{tj}$  and has therefore a nonconvex feasible area.

Next, we linearize the binary bilinear term  $y_{lj} y_{tj}$  by introducing the variables  $z_{lt}^j$  and the linear inequalities (20a)-(20d) in the set  $\mathcal{M}_{z_{lt}^j}$  which ensures that  $z_{lt}^j := y_{lj} y_{tj}$  and gives the equality:

$$4U_j^2 - \sum_{l \in I_j} (\lambda_l)^2 U_j^2 y_{lj} \tilde{S}_{lj}^2 - 2 \sum_{l,t \in D_j} \lambda_l \lambda_t U_j^2 z_{lt}^j \tilde{S}_{lj} \tilde{S}_{tj} = \sum_{l \in I_j} (\lambda_l)^2 y_{lj} \tilde{S}_{lj}^2 \tilde{S}_{lj} + 2 \sum_{l,t \in D_j} \lambda_l \lambda_t z_{lt}^j \tilde{S}_{lj}^2 \tilde{S}_{tj}, \quad j \in J \tag{35}$$

To linearize the remaining bilinear terms  $U_j^2 y_{lj}$  and  $U_j^2 z_{lt}^j$  in (35), we respectively use the inequalities (21a)-(21d) and (22a)-(22d) in  $\mathcal{M}_{\mu_{lj}^2}$  and  $\mathcal{M}_{\tau_{lt}^j}$  to ensure  $\mu_{lj}^2 := U_j^2 y_{lj}$  and  $\tau_{lt}^j := U_j^2 z_{lt}^j$ , which gives us, in fine, a mixed-integer linear feasible set equivalent to (27).

Having linearized the bilinear terms in (26) and (27), we do now the same for the trilinear terms  $\gamma_j^1 y_{ij} U_j^1$  and  $\gamma_j^2 y_{ij} U_j^2$  in the objective function (28). First, since  $\mu_{ij}^m = U_j^m y_{ij}$ , the trilinear terms can be reduced to the bilinear terms  $\gamma_j^1 \mu_{ij}^1$  and  $\gamma_j^2 \mu_{ij}^2$ . Introducing the variables  $\omega_{ij}^m$  such that  $\omega_{ij}^m := \gamma_j^m \mu_{ij}^m$  due to the McCormick inequalities (23a)- (23d) in the set  $\mathcal{M}_{\omega_{ij}^m}$ , we have  $\omega_{ij}^m = \gamma_j^m \mu_{ij}^m = \gamma_j^m y_{ij} U_j^m$  and substituting  $\omega_{ij}^m$  for  $\gamma_j^m y_{ij} U_j^m$  gives a linear objective function and completes the proof.  $\square$

In Appendix B, we give the objective formulation of problem **R – MILP** for a small network.

We shall now demonstrate in Theorem 7 that the linearization approach proposed above for an  $M/G/K$  queueing system with variable number of servers (capacity)  $K$  limited from above to 2 can be extended to any  $M/G/K$  system with finite variable capacity  $K$ . We first introduced two Propositions that will be used in the proof of Theorem 7.

**Proposition 5** *Let  $y \in \{0, 1\}^n$ . The polynomial set  $\{(y, z) \in \{0, 1\}^n \times [0, 1] : z = \prod_{i=1}^n y_i\}$  can be equivalently represented with the MILP set defined by:*

$$\{(y, z) : z \geq 0, z \geq \sum_{i=1}^n y_i - n + 1, z \leq y_i, i = 1, \dots, n\}.$$

**Proposition 6** *Let  $x \in [0, \bar{x}]$ ,  $y \in \{0, 1\}^n$ . The polynomial set  $\{(x, y, z) \in [0, \bar{x}] \times \{0, 1\}^n \times [0, \bar{x}] : z = x \prod_{i=1}^n y_i\}$  can be equivalently represented with the MILP set defined by:*

$$\{(x, y, z) : z \geq 0, z \geq x - \bar{x}(n - \sum_{i=1}^n y_i), z \leq \bar{x}y_i, z \leq x, i = 1, \dots, n\}.$$

**Theorem 7** *A stochastic network design model of form **R – BFP** that minimizes the average response time of a network of  $M/G/K_j$  queueing systems with variable and finitely bounded number of servers  $K_j$  is always MILP-representable.*

**Proof:** Each fractional term (25) ( $m \in \{1, M\}$ ) in the objective function of **R – BFP** can be equivalently reformulated as:

$$\frac{\gamma_j^m \sum_{l \in I_j} \lambda_l y_{lj} \tilde{S}_{lj}^2 (\sum_{l \in I_j} \lambda_l y_{lj} \tilde{S}_{lj})^{m-1}}{2((m-1)!(m - \sum_{l \in I_j} \lambda_l y_{lj} \tilde{S}_{lj})^2 \sum_{n=0}^{m-1} \frac{(\sum_{l \in I_j} \lambda_l y_{lj} \tilde{S}_{lj})^n}{n!} + (m - \sum_{l \in I_j} \lambda_l y_{lj} \tilde{S}_{lj})(\sum_{l \in I_j} \lambda_l y_{lj} \tilde{S}_{lj})^m)}. \quad (36)$$

Let introduce an auxiliary continuous variable  $V_j^m \in [0, \bar{V}_j^m]$  for each term ( $m$ ) in (36):

$$V_j^m = \frac{\gamma_j^m \sum_{l \in I_j} \lambda_l y_{lj} \tilde{S}_{lj}^2 (\sum_{l \in I_j} \lambda_l y_{lj} \tilde{S}_{lj})^{m-1}}{2((m-1)!(m - \sum_{l \in I_j} \lambda_l y_{lj} \tilde{S}_{lj})^2 \sum_{n=0}^{m-1} \frac{(\sum_{l \in I_j} \lambda_l y_{lj} \tilde{S}_{lj})^n}{n!} + (m - \sum_{l \in I_j} \lambda_l y_{lj} \tilde{S}_{lj})(\sum_{l \in I_j} \lambda_l y_{lj} \tilde{S}_{lj})^m)} \quad (37)$$

Substituting  $V_j^m$  for (36) in the objective function (12a), problem **R – BFP** becomes:

$$\min \sum_{i \in I} \sum_{j \in J_i} \frac{y_{ij} d_{ij} \lambda_i}{v \sum_{l \in I} \lambda_l} + \sum_{i \in I} \sum_{j \in J_i} \sum_{m=1}^M \frac{y_{ij} \lambda_i V_j^m}{\sum_{l \in I} \lambda_l} \quad (38a)$$

s.to  $(x, y, \gamma) \in \mathcal{BL}$

$$\begin{aligned} & \underbrace{V_j^m (m-1)! (m - \sum_{l \in I_j} \lambda_l y_{lj} \tilde{S}_{lj})^2 \sum_{n=0}^{m-1} \frac{(\sum_{l \in I_j} \lambda_l y_{lj} \tilde{S}_{lj})^n}{n!}}_{T1} + \underbrace{V_j^m (m - \sum_{l \in I_j} \lambda_l y_{lj} \tilde{S}_{lj}) (\sum_{l \in I_j} \lambda_l y_{lj} \tilde{S}_{lj})^m}_{T2} \\ & = 1/2 \underbrace{\gamma_j^m \sum_{l \in I_j} \lambda_l y_{lj} \tilde{S}_{lj}^2 (\sum_{l \in I_j} \lambda_l y_{lj} \tilde{S}_{lj})^{m-1}}_{T3}, \quad j \in J, m \in M \end{aligned} \quad (38b)$$

It can be seen from the above that:

- The objective function includes bilinear terms involving the product of a continuous variable  $V_j^m$  and a binary variable  $y_{ij}$ . These bilinear terms can be linearized using the approach described in Proposition 6.
- The expressions T1 and T2 in (38b) include both polynomial terms of degree  $(m + 2)$  with monomials involving the product of a continuous variable by up to  $(m + 1)$  binary variables. These polynomial terms can be linearized using the approach described in Proposition 6.
- The expression T3 in the right-side of (38b) includes polynomial terms of degree  $(m + 1)$  involving products of  $m + 1$  binary variables. These polynomial terms can be linearized using the approach described in Proposition 5.

This shows that both the objective function and each constraint (36) can be linearized regardless of the value of  $M$ , which is the result that we set out to prove.  $\square$

## 5 Algorithmic Method

Even though **R-MILP** is an MILP problem, its solution remains nonetheless a challenge owing to its combinatorial nature and size. Linearization methods suffer from two possible drawbacks. First, they require the introduction of many decision variables and constraints and second the resulting continuous relaxations can be very loose (i.e., some of the added constraints are big-M ones). To palliate these issues, we use the concepts of lazy constraints, valid inequalities, and optimality-based cuts to devise outer approximation methods whose efficiency and scalability is demonstrated in Section 6.3.

### 5.1 Outer Approximation Algorithm with Lazy Constraints

While instances of the special variant of model **R-MILP** when the maximal number  $M$  of drones at each DB is fixed and equal to 1 (i.e., each open DB is an M/G/1 system) can be solved, preliminary experiments reveal that state-of-the-art solvers are however unable to solve, within 1 hour, the root node

of the continuous relaxation of the moderate-sized **R-MILP** problem instances for  $M \geq 2$ . To overcome this issue, we derive an MILP relaxation for problem **R – MILP** using *lazy constraints* (see, e.g., [32, 35]) and embed it in an outer approximation algorithm. The motivation is to alleviate the issue caused by the significantly lifted decision and constraint space due to the linearization method.

A *lazy constraint* is an integral part of the actual constraint set (which could lead to invalid solutions in its absence) and is unlikely to be binding at the optimal solution. Instead of incorporating all lazy constraints in the formulation, they are grouped in a pool and are at first removed from the constraint set before being (possibly) iteratively and selectively reinstated on an as-needed basis. The targeted benefit is to obtain a reduced-size relaxation or outer approximation problem, which is quicker to solve and tight. One should err on the side of caution when deciding which constraints are set up as lazy. Indeed, the inspection of whether a lazy constraint is violated is carried out each time a new incumbent solution for the outer approximation problem is found and the computational overheads consecutive to the possible need to reintroduce violated lazy constraints in the constraint set can be significant.

Within this approach, the reduced-size relaxation is solved at each node of the tree. Each time a new incumbent solution is found, a verification is made to check whether any lazy constraint is violated. If it is the case, the incumbent integer solution is discarded and the violated lazy constraints are (re)introduced in the constraint set of all unprocessed nodes of the tree, thereby cutting off the current solution.

We define here the linearization constraints (20a)-(20d) and (22a)-(22d) in the sets  $\mathcal{M}_{z_{it}^j}$  and  $\mathcal{M}_{\tau_{it}^j}$  as lazy constraints. The motivation for this choice is threefold and guided by: the results of preliminary numerical tests, the very large number  $\sum_{j \in J} |I_j| \cdot (|I_j| - 1)/2$  of such constraints, and the fact that (22a)-(22d) are not always needed, i.e., they only play a role if two drones are placed at the same DB.

The following notations are used. Let  $\mathcal{O}$  denote the set of open nodes in the tree. We call iteration a node of the branch-and-bound tree at which the optimal solution of the continuous relaxation is integer-feasible. Let  $\mathcal{C}$  be the entire constraint set of problem **R – MILP** (see Theorem 4),  $\mathcal{L}_k$  be the set of lazy constraints at node  $k$ ,  $\mathcal{V}_k^L$  be the set of violated lazy constraints at  $k$ , and  $\mathcal{A}_k := \mathcal{C} \setminus \mathcal{L}_k$  be the set of active constraints at  $k$ , i.e., the set of constraints of the reduced-size outer approximation problem **OA – MILP<sub>k</sub>**. The composition of the sets vary across the algorithmic process.

The outer approximation algorithm OA is designed as follows. At the root node ( $k = 0$ ), we have:

$$\mathcal{L}_0 := \{(20a) - (20d); (22a) - (22d)\}. \quad (39)$$

$$\mathcal{A}_0 := \{\mathcal{BL}; (24b) - (24c); \mathcal{M}_{\mu_{ij}^m}; \mathcal{M}_{\omega_{ij}^m}\}. \quad (40)$$

$$\mathcal{V}_0 := \emptyset. \quad (41)$$

At any node  $k$ , the reduced-size relaxation (outer approximation) problem **OA – MILP<sub>k</sub>** is solved:

$$\mathbf{OA - MILP}_k : \min (24a) \quad \text{s.to} \quad (x, y, \gamma, z, U, \mu, \tau, \omega) \in \mathcal{A}_k\}.$$

Two cases are distinguished depending on the optimal solution  $X_k^*$  of the continuous relaxation of **OA – MILP<sub>k</sub>**:

(1) If  $X_k^*$  is fractional, we introduce branching linear inequalities to cut off the fractional nodal optimal solution and we continue the branch-and-bound process.

(2) If  $X_k^*$  is an integer-valued solution with better objective value than the one of the current incumbent, we check for possible violation of the current lazy constraints:

- If some constraints are violated by  $X_k^*$ , they are inserted in  $\mathcal{V}_k^L \subseteq \mathcal{L}_k$  and  $X_k^*$  is discarded. The lazy and active constraint sets of each open node  $o \in \mathcal{O}$  are updated as follows:

$$\mathcal{L}_o \leftarrow \mathcal{L}_o \setminus \mathcal{V}_k^L \quad \text{and} \quad \mathcal{A}_o \leftarrow \mathcal{A}_o \cup \mathcal{V}_k^L.$$

- If no lazy constraint is violated,  $X_k^*$  becomes the incumbent solution and the node is pruned.

The above process terminates when all nodes are pruned. The verification of the possible violation of the lazy constraints is carried out within a callback function, which is not performed at each node of the tree, but only when a better integer-valued feasible solution is found. The use of the lazy constraints within the outer approximation procedure is pivotal in the proposed method as shown in Section 6.3. The pseudo-code of the algorithm is given below in Algorithm 1.

---

**Algorithm 1** Outer Approximation (OA)

---

**Part 1 (Initialization):**  $\mathcal{L}_0 := \{(20a) - (20d); (22a) - (22d)\}$ ;  $\mathcal{A}_0 := C \setminus \mathcal{L}_0$ ;  $\mathcal{V}_0^L = \emptyset$ .

**Part 2 (Iterative Procedure):** At node  $k$ :

**Step 1: Solution of nodal relaxation problem OA – MILP<sub>k</sub>:**

$$\text{OA – MILP}_k : \min (24a) \quad \text{s.to} \quad (x, y, \gamma, z, U, \mu, \tau, \omega) \in \mathcal{A}_k.$$

**Step 2: Set Update:**

- If the objective value corresponding to  $X_k^*$  is not better than that of the incumbent, the node is pruned.
- If the objective value corresponding to  $X_k^*$  is better than that of the incumbent, then:
  - If  $X_k^*$  is fractional, introduce branching inequalities cutting off  $X_k^*$  and move to next node.
  - If  $X_k^*$  is integer-valued, check for possible violation of lazy constraints:
    - \* If  $X_k^*$  violates any constraint in  $\mathcal{L}_k$ :
      - Move violated lazy constraints to  $\mathcal{V}_k^L$  and discard  $X_k^*$ .
      - Update sets of lazy and active constraints for each open node  $o \in \mathcal{O}$ :

$$\mathcal{L}_o \leftarrow \mathcal{L}_o \setminus \mathcal{V}_k^L \quad \text{and} \quad \mathcal{A}_o \leftarrow \mathcal{A}_o \cup \mathcal{V}_k^L.$$

- \* If  $X_k^*$  does not violate any constraint in  $\mathcal{L}_k$ ,  $X_k^*$  becomes the incumbent and node  $k$  is pruned.

**Part 3 (Termination):** The algorithm stops when  $\mathcal{O} = \emptyset$ .

---

## 5.2 Outer Approximation Branch-and-Cut Algorithm

The linearization approach involves the introduction of big-M constraints which typically lead to loose continuous relaxations. To tighten the continuous relaxation, we derive valid inequalities and optimality-based cuts. Combining them with the outer approximation method OA, we obtain an outer approximation branch-and-cut algorithm OA-B&C.

A valid inequality does not rule out any feasible integer solutions but cuts off fractional solutions feasible for the continuous relaxation problem. In essence, it pares away at the space between the linear and integer hulls, thereby providing a tighter formulation. In contrast to lazy constraints, a valid inequality is inserted in the formulation if the optimal solution of the continuous relaxation at any node is fractional and violates this valid inequality. We shall now derive two types of valid inequalities.

The valid inequalities (42) reflect the fact that if either one of the variables  $U_j^1$  or  $U_j^2$  representing the expecting delay time is positive then at least one drone is positioned at DB  $j$  and that if DB  $j$  is not active, then the variables  $U_j^m, m = 1, 2$  are equal to 0.

**Proposition 8** Let  $U_j^m \in [0, \bar{U}_j^m], m = 1, 2$ . The linear constraints

$$\gamma_j^1 + \gamma_j^2 \geq U_j^m / \bar{U}_j^m, \quad j \in J, m = 1, 2 \quad (42)$$

are valid inequalities for problem **R-MILP**.

**Proof:** If for any  $m \in \{1, 2\}$ , we have  $U_j^m / \bar{U}_j^m > 0$ , which means  $U_j^m > 0$  and  $U_j^m / \bar{U}_j^m \leq 1$  since  $U_j^m \in [0, \bar{U}_j^m]$ , this implies in turn  $\gamma_j^1 + \gamma_j^2 = 1$ . This forces either  $\gamma_j^1$  or  $\gamma_j^2$  to take value 1, which does not cut off any integer solution. If there is no DB open at  $j$ , i.e.,  $x_j = 0 = \gamma_j^1 + \gamma_j^2$ , then  $y_{i,j} = 0, i \in J_i$  due to (11d) and  $U_j^1 = U_j^2 = 0$  due to (26) and (27), which is valid for (42).  $\square$

The valid inequalities (43) reflect that the queueing delay at a DB  $j$  is a decreasing function of the number of drones positioned at this DB.

**Proposition 9** The linear constraints

$$U_j^1 \geq U_j^2, \quad j \in J \quad (43)$$

are valid inequalities for problem **R-MILP**.

**Proof:** If no DB is set up at location, we have  $U_j^1 = U_j^2 = 0$  due to (26) and (27), and (43) holds.

If a DB is set up at location  $j$ , we have from (27) the first equality below:

$$U_j^2 = \frac{\sum_{l \in I_j} \lambda_l y_{lj} \tilde{S}_{lj}^2 \sum_{l \in I_j} \lambda_l y_{lj} \tilde{S}_{lj}}{(2 - \sum_{l \in I_j} \lambda_l y_{lj} \tilde{S}_{lj})^2 + (2 - \sum_{l \in I_j} \lambda_l y_{lj} \tilde{S}_{lj})^2 \sum_{l \in I_j} \lambda_l y_{lj} \tilde{S}_{lj} + (2 - \sum_{l \in I_j} \lambda_l y_{lj} \tilde{S}_{lj})(\sum_{l \in I_j} \lambda_l y_{lj} \tilde{S}_{lj})^2} \quad (44)$$

$$\leq \frac{\sum_{l \in I_j} \lambda_l y_{lj} \tilde{S}_{lj}^2 \sum_{l \in I_j} \lambda_l y_{lj} \tilde{S}_{lj}}{(2 - \sum_{l \in I_j} \lambda_l y_{lj} \tilde{S}_{lj})^2 \sum_{l \in I_j} \lambda_l y_{lj} \tilde{S}_{lj}} = \frac{\sum_{l \in I_j} \lambda_l y_{lj} \tilde{S}_{lj}^2}{(2 - \sum_{l \in I_j} \lambda_l y_{lj} \tilde{S}_{lj})^2} \quad (45)$$

$$\leq \frac{\sum_{l \in I_j} \lambda_l y_{lj} \tilde{S}_{lj}^2}{2 - \sum_{l \in I_j} \lambda_l y_{lj} \tilde{S}_{lj}} \quad (46)$$

$$\leq \frac{\sum_{l \in I_j} \lambda_l y_{lj} \tilde{S}_{lj}^2}{1 - \sum_{l \in I_j} \lambda_l y_{lj} \tilde{S}_{lj}} = U_j^1. \quad (47)$$

The validity of the first inequality is implied by the steady-state requirement (11b) according to which we have either  $1 - \sum_{l \in I_j} \lambda_l y_{lj} \tilde{\mathcal{S}}_{lj} \geq 0$  when  $\gamma_j^1 = 1$  or  $2 - \sum_{l \in I_j} \lambda_l y_{lj} \tilde{\mathcal{S}}_{lj} \geq 0$  when  $\gamma_j^2 = 1$ . It follows immediately that the denominator of (44) is larger than the one in (45). Since the numerators are the same in (44) and (45), we have (45)  $\geq$  (44). Next, observe that (26) implies that we have always  $1 \geq \sum_{l \in I_j} \lambda_l y_{lj} \tilde{\mathcal{S}}_{lj}$  since otherwise the nonnegative auxiliary variable  $U_j^1$  would be negative. This in turn implies  $2 - \sum_{l \in I_j} \lambda_l y_{lj} \tilde{\mathcal{S}}_{lj} \geq 1$  and  $(2 - \sum_{l \in I_j} \lambda_l y_{lj} \tilde{\mathcal{S}}_{lj})^2 \geq 2 - \sum_{l \in I_j} \lambda_l y_{lj} \tilde{\mathcal{S}}_{lj} \geq 1$ . Therefore, the denominator of (45) is larger than the one of (46) and (46)  $\geq$  (45). Similarly, the third inequality is valid since  $2 - \sum_{l \in I_j} \lambda_l y_{lj} \tilde{\mathcal{S}}_{lj} > 1 - \sum_{l \in I_j} \lambda_l y_{lj} \tilde{\mathcal{S}}_{lj}$  which implies (47)  $>$  (46) and allows us to conclude that  $U_j^2 \leq U_j^1$ .  $\square$

Besides valid inequalities, we also derive optimality-based cuts (see Proposition 10) which cut off integer feasible solutions that are not optimal or in a way that *not all* optimal solutions are removed. The proposed optimality-based cuts (48) state that the opening of a DB at location  $j$  is required if and only if either one or two drones are positioned at  $j$ .

**Proposition 10** *The linear constraints*

$$\gamma_j^1 + \gamma_j^2 = x_j, \quad j \in J \quad (48)$$

*are optimality-based cuts for problem R-MILP.*

**Proof:** The sum  $\gamma_j^1 + \gamma_j^2$  can never exceed 1 due to (12e). If  $\gamma_j^1 + \gamma_j^2 = 1$ , it follows from (12c) that  $x_j = 1$ . If  $\gamma_j^1 + \gamma_j^2 = 0$ , (12c) allows  $x_j$  to be equal to 0 or 1. However, (48) cuts off the integer solutions  $(x_j, \gamma_j^1, \gamma_j^2) = (1, 0, 0), j \in J$ , which are not optimal and do not give a better objective value than  $(x_j, \gamma_j^1, \gamma_j^2) = (0, 0, 0), j \in J$ .  $\square$

While deceptively simple, the incorporation of the proposed valid inequalities and optimality-based cuts in the outer approximation algorithm branch-and-cut algorithm OA-B&C has a very significant computational impact as shown in Section 6.3.1.

The set  $\mathcal{B}$  of optimality-based cuts (48) are added to the pool of lazy constraints (39):

$$\mathcal{L}'_0 := \mathcal{L}_0 \cup \mathcal{B}. \quad (49)$$

The valid inequalities are grouped in a user cut pool.  $\mathcal{U}_k$  be the user cut set (of valid inequalities) at the root node  $k = 0$ :  $\mathcal{U}_0 := \{(42) - (43)\}$  while  $\mathcal{V}_k^U$  is the set of valid inequalities violated by the fractional optimal solution of the continuous relaxation at node  $k$ .

The outer approximation branch-and-cut algorithm OA-B&C is structured as follows. The two families of valid inequalities (42) and (43) are derived up-front, incorporated into a pool of user cuts, and applied and checked dynamically each time the nodal optimal solution  $X_k^*$  is fractional through a user cut callback implemented in GUROBI. If  $X_k^*$  is fractional, the user callback is applied and the violated – if any – valid inequalities in the current user cut pool  $\mathcal{U}_k$  are added to the active constraint set of each open node  $o \in \mathcal{O}$  (thereby cutting off  $X_k^*$ ) and are removed from the user cut pool:

$$\mathcal{U}_o \leftarrow \mathcal{U}_o \setminus \mathcal{V}_k^U \quad \text{and} \quad \mathcal{A}_o \leftarrow \mathcal{A}_o \cup \mathcal{V}_k^U.$$

If no inequality in  $\mathcal{U}_k$  is violated by  $X_k^*$ , then two branching constraints are entered to cut off  $X_k^*$  and the next open node is processed. Note that, if  $X_k^*$  is integer feasible, the user cut callback is not applied. The algorithm stops when the set of unprocessed nodes becomes empty. The pseudo-code of the algorithmic method OA-B&C follows.

---

**Algorithm 2** Outer Approximation Branch-and-Cut Algorithm (OA-B&C)

---

**Part 1 (Initialization):**  $\mathcal{L}_0 := \{(20a) - (20d); (22a) - (22d)\}$ ;  $\mathcal{B} = \{(48)\}$ ;  $\mathcal{L}'_0 := \mathcal{L}_0 \cup \mathcal{B}$ ;  $\mathcal{U}_0 := \{(42); (43)\}$ ;  $\mathcal{A}_0 := C \setminus \mathcal{L}_0$ ;  $\mathcal{V}_0^L = \emptyset$ ;  $\mathcal{V}_0^U = \emptyset$ .

**Part 2 (Iterative Procedure): At node  $k$**

**Step 1: Solution of nodal relaxation problem:**

$$\text{OA - MILP}_k : \min (24a) \quad \text{s.to} \quad (x, y, \gamma, z, U, \mu, \tau, \omega) \in \mathcal{A}_k .$$

**Step 2: Set Update:**

- **If the objective value corresponding to  $X_k^*$  is not better than that of the incumbent**, the node is pruned.
- **If the objective value corresponding to  $X_k^*$  is better than that of the incumbent**, then:
  - **If  $X_k^*$  is fractional**, apply user callback:
    - \* If  $X_k^*$  violates any constraint in  $\mathcal{U}_k$ :
      - Move violated constraints to  $\mathcal{V}_k^U$  and discard  $X_k^*$ .
      - Update sets of user cuts and active constraints for each open node  $o \in \mathcal{O}$

$$\mathcal{U}_o \leftarrow \mathcal{U}_o \setminus \mathcal{V}_k^U \quad \text{and} \quad \mathcal{A}_o \leftarrow \mathcal{A}_o \cup \mathcal{V}_k^U .$$

- \* If no valid inequality in  $\mathcal{U}_k$  is violated by  $X_k^*$ , then branching constraints are entered to cut off  $X_k^*$  and the next open node is processed.
- **If  $X_k^*$  is integer-valued**, update the sets of lazy and active constraints according to Step 2 (Part 2) of Algorithm 1.

**Part 3 (Termination):** The algorithm stops when  $\mathcal{O} = \emptyset$ .

---

## 6 Data-Driven Tests and Insights

To demonstrate the benefits and applicability of the proposed approach and validate its computational efficiency, we conduct extensive numerical tests using the real-life opioid overdose data described in Section 6.1. Section 6.2 provides practical insights related to response time, chance of survival, quality-adjusted life year (QALY), and costs, and attests the applicability and robustness of the approach through a cross-validation analysis. Section 6.3 evaluates the computational efficiency and tractability of the reformulation and algorithmic framework.

### 6.1 Real-life Opioid Overdose Data

The dataset used in the tests describes the opioid overdose incidents in the city of Virginia Beach and is publicly available [21]. The data were collected through multiple sources, including the OpenVB data portal, Freedom of Information Act requests to the government of Virginia Beach, and public reports. The data collection process was validated by the Virginia Beach officials.

The dataset contains all dispatch records for OTRs from the second quarter of 2018 to the third

quarter of 2019, which amounts to a total of 733 data points (overdoses). Each record has four fields including the time at which the request was received by the EMS, the response time, i.e, time between the reception of the request and the arrival of the EMS personnel on the scene, and the location (i.e., latitude and longitude) of the request. The dataset also provides the location of the twenty-six established EMS facilities (i.e., fire, police, and EMS stations) that can be selected as drone bases. As in [11], we consider that drones can travel at a speed of 27.8 meters per second (m/s) and take 10 seconds to take off and to land. We use 25 minutes as the expected non-travel service time which includes the time to administer the naloxone at the overdose location and to recharge and prepare the drone for the next assignment.

We have conducted a grid search in order to identify the minimal size of the drone network to be able to respond to all OTRs. This revealed that the drone network should include at least  $p = 11$  drones and does not require more than  $q = 10$  DBs. Thereafter, we refer to “base scenario” the case in which the drone response network allows for the opening of ten DBs and the deployment of eleven drones.

## 6.2 Interplay Between Response Time, Survival Chance, QALY, and Delivery Mode

Section 6.2.1 analyzes the reduction in the response time attributable to the drone network, the applicability and robustness of the proposed approach, and the spatio-temporal adjustments in the OTRs and drone network. Section 6.2.2 investigates the increase in the chance of survival of an overdose victim and the expected number of lives saved. Section 6.2.3 quantifies the impact on the quality-adjusted life year and performs a cost analysis.

### 6.2.1 Response Time Reduction and Network Robustness

We analyze here how the response time, a critical metric for EMSs, can be improved by using drones. We first carry out an in-sample analysis before cross-validating the results and assessing, using out-of-sample data, the stability of the results and the robustness of the designed networks.

**In-sample analysis:** We consider quarterly data sets of opioid overdose incidents which we denote 2018Q2 (2018’s second quarter), 2018Q3, 2018Q4, 2019Q1, and 2019Q2. We consider the base scenario in which one can open up to 10 DBs and deploy 11 drones ( $q = 10, p = 11$ ). To estimate the in-sample performance and response times of the drone network, we solve the network design problem **R – MILP** associated to a quarterly training dataset, retrieve its optimal solution and value, and calculate the average response time across all opioid overdoses in the corresponding quarter.

Table 1 shows the average response times on the training sets with the proposed drone network and those obtained in Virginia Beach with their current ambulance-based EMS network, which highlights the significant decrease in the average response time enabled by the drone network (i.e., 1 minute and 19 seconds versus 8 minutes and 56 seconds for the ambulance network). As compared to the current ambulance network, the drone network reduces the response time by 85.35% on average. The reduction of the response time is stable across all quarters and is not due to chance.

Training Set	Response Time (minutes)		
	Drone Networks	VB Ambulance Networks	Time Reduction
2018Q2	1.34	8.77	84.72%
2018Q3	1.36	9.02	84.92%
2018Q4	1.25	9.42	86.73%
2019Q1	1.29	8.56	84.93%
Quarter Average	1.31	8.94	85.35%

Table 1: Response Times in Quarterly Training Sets ( $q = 10, p = 11$ )

**Out-of-sample analysis:** We now carry out a cross-validation analysis to assess how the training set-based networks perform on out-of-sample data that were not used in the design of the network. Using the five sets of quarterly data, we create four pairs of consecutive quarterly sets, e.g., (2018Q2 and 2018Q3), where the first one is the training set (2018Q2) and the second one is the testing set (2018Q3). Table 2 describes the size of the data sets. The number of OTRs in each quarterly dataset is  $|I|$ .

Pairs of Sets	Training Sets	$ I $ - Training	Testing Sets	$ I $ - Testing
(2018Q2, 2018Q3)	2018Q2	173	2018Q3	131
(2018Q3, 2018Q4)	2018Q3	131	2018Q4	120
(2018Q4, 2019Q1)	2018Q4	120	2019Q1	138
(2019Q1, 2019Q2)	2019Q1	138	2019Q2	171

Table 2: Data Summary

For each pair of training and testing sets, we use the training set only to build the network: we solve the network design problem **R – MILP** associated to the training set and retrieve its optimal solution. This provides us with the training set-based optimal configuration of the network, namely the optimal location  $x^*$  of the opened DBs and the optimal number of drones (which can be inferred from the variables  $\gamma^*$ ) to be stationed at each DB. Using the optimal location decisions for the training set-based network, we then solve an assignment problem corresponding to the testing set, which is a "reduced" form of problem **R – MILP** in which the variables  $x$  and  $\gamma$  are fixed to their optimal values for the training set:  $x := x^*$  and  $\gamma := \gamma^*$ . The optimal solution of the testing set-based assignment provides the optimal drone-dispatching decisions for OTRs based on the training set-based network configuration, which allows us to calculate the individual and average out-of-sample (testing set) response times to OTRs.

The results are displayed in Table 3. The cross-validation analysis confirms the results envisioned in the in-sample analysis. The network configurations for the training sets reduces in a striking manner the out-of-sample response time. Across all quarters, the average out-of-sample response time is of 1 minute and 26 seconds while it amounts to 9 minutes and 19 seconds for the ambulance network in Virginia Beach. This corresponds to a 84.57% reduction in the average response time. The quarterly average response times are stable and similar to those obtained in the in-sample analysis.

Training/Testing Data	Testing Quarter Response Time (min.)		
	Drone Network	VB Ambulance Network	Time Reduction
2018Q2 / 2018Q3	1.51	9.02	83.26%
2018Q3 / 2018Q4	1.38	9.42	85.35%
2018Q4 / 2019Q1	1.48	8.56	82.71%
2019Q1 / 2019Q2	1.38	10.27	86.56%
Quarter Average	1.43	9.32	84.57%

Table 3: Out-of-Sample Response Times for Testing Quarters ( $q = 10, p = 11$ )

The last part of this subsection illustrates the spatio-temporal variability of the OTRs and its impact on the optimal configuration of the drone network. Figure 1 presents the distribution of the OTRs and the configurations of the drone-based networks for two consecutive quarters, i.e., 2018’s second (2018Q2) and third (2018Q3) quarters. In both networks, ten DBs are opened; one drone is located at nine of the DBs operating as M/G/1 systems while the last one operates as an M/G/2 system with two available drones. Comparing the two networks, one can see that the location of most DBs remains unchanged over time. One noticeable change is that, in the 2018Q3 network a new DB is opened in the southwest of the map to cover an increased number of OTRs in this remote area. Another change is the new DB in the North. In Figure (1b), the two new DBs are surrounded by a rectangle while the two closed ones are circled. The aforementioned location changes reflect the impact of the spatial uncertainty on the optimal configuration of the network. In that regard, the flexibility, ease and limited cost to open (close) a DB [56] are important to be able to adapt to geographical changes in the occurrence of OTRs.

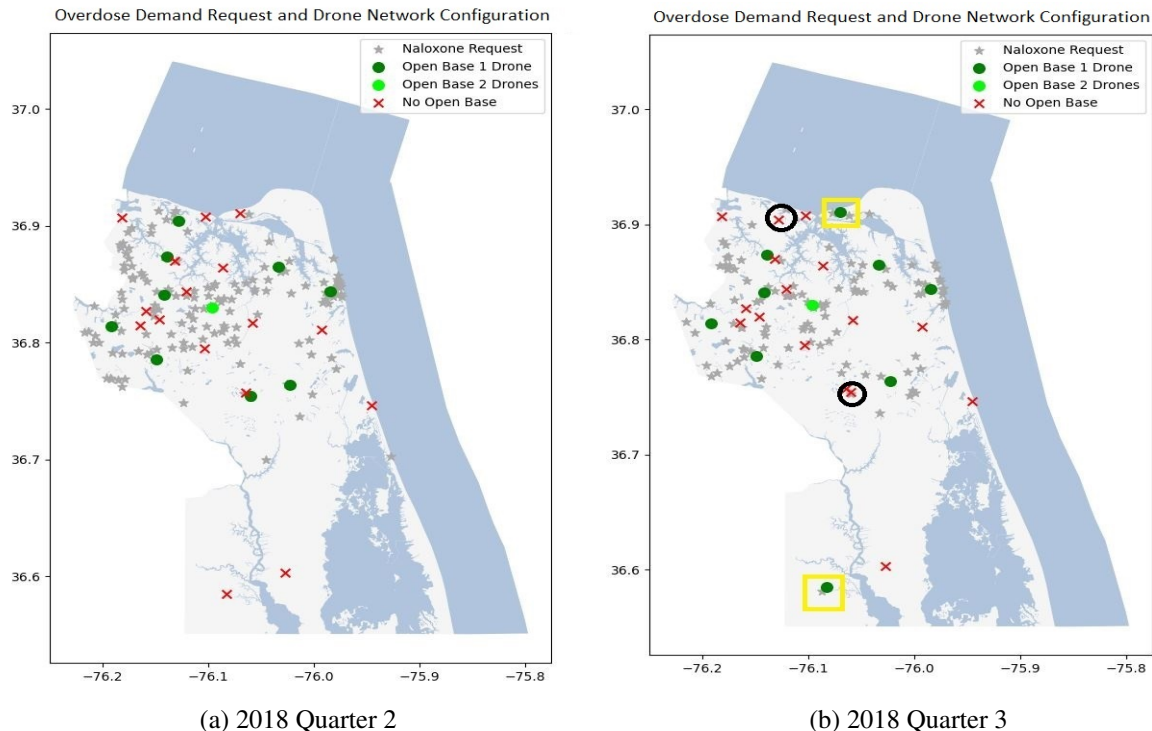


Figure 1: OTR Demand and Drone Network Configuration

## 6.2.2 Impact on Probability of Survival

The goal of this section is to quantify the benefits of the reduced response time afforded by the drone network (Section 6.2.1) on the survival chance of overdose victims. Since we are not aware of any functional relationship between response time and survival probability of an opioid overdose victim, we hereby employ an indirect two-step approach using known survival functions for cardiac arrests. The main reason for this is that many overdoses lead to cardiac arrests. Indeed, the increase in cardiac arrest caused by opioid medications is said to be *”the most dramatic manifestation of opioid use disorder“* [23]. Step 1: We calculate the number of out-of-hospital cardiac arrests (OHCA) resulting from an opioid overdose and use the statistics reported by Dezfulian et al. [23] which indicate that 15% of opioid overdoses lead to an OHCA. As shown in the last column in Table 2, 560 overdose incidents are reported in Virginia Beach over one year (i.e., from 2018Q3 to 2019Q2), leading to an estimated (see [23]) number of 84 overdose-associated OHCA.

Step 2: Using three known survival functions for OHCA (see Table 4) that define the survival probability  $f(x)$  to an OHCA as either a semi-continuous or a logistic function of the response time  $x$ , we calculate the estimated probability of survival for overdose-associated OHCA with the drone network and with the EMS ambulance network in use in Virginia Beach. This allows us in turn to derive the differences in the survival chance and in the expected number of saved lives with the drone and ambulance networks.

Author	Function Type	$f(x)$
Bandara et al. [3]	Semi-continuous	$\max [0.594 - 0.055x, 0]$
De Maio et al. [22]	Logistic	$(1 + e^{0.679+0.262x})^{-1}$
Chanta et al. [18]	Logistic	$(1 + e^{-0.015+0.245x})^{-1}$

Table 4: Survival Functions for OHCA

As shown in the last row of Table 3, the out-of sample average response time (over one year) for the drone network is 1.43 minutes whereas the current EMS network takes 9.32 minutes for the same period. Figure 2 shows the survival probability – for the three survival functions described in Table 4 – of the overdose-associated OHCA obtained with the drone and with Virginia Beach’s ambulance EMS network. The difference between the two networks is striking. The drone network significantly increases the patients’ survival probability with each survival function. The chance of survival with the drone network is indeed 5.37 (resp., 5.5 and 3.66) times larger than the one with Virginia Beach’s current ambulance network as estimated by the survival function [3] (resp., [22], and [18]).

Table 5 displays the survival probability and the expected number of patients surviving an overdose-associated OHCA in Virginia Beach for the four quarters considered. These statistics are provided for the drone network (column 4) and for Virginia Beach’s current ambulance network (column 5) as benchmark. One can see that the drone network is extremely beneficial and increases the number of survivors by 637.5%, (resp., 650% and 466.7%) using the survival function [3] (resp.[22] and [18]).

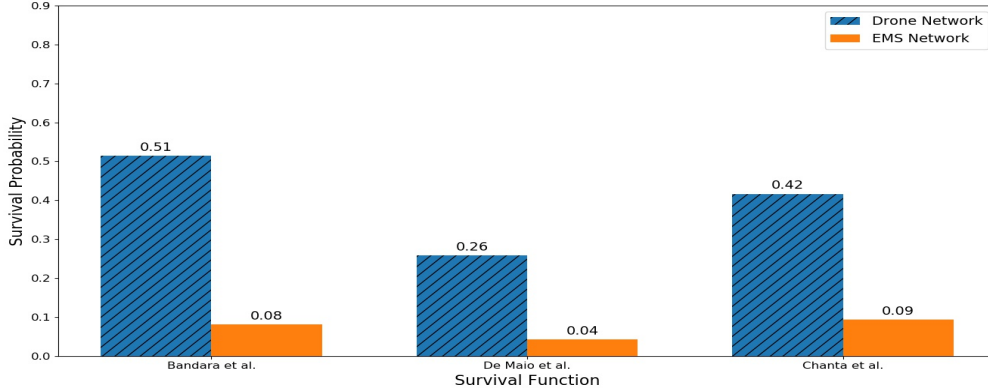


Figure 2: Survival Probability for Drone Network and Virginia Beach Ambulance Network

Total Number of Overdoses	Overdose-related OHCAs	Survival Function	Survival Prob. / No. of Survivors	
			Drone Network	EMS Network
560	84	Bandara et al. [3]	51% / 42	8% / 6
		De Maio et al. [22]	26% / 21	4% / 3
		Chanta et al. [18]	42% / 35	9% / 7

Table 5: Expected Saved Lives with Drone Network

Table 5 shows that, depending on the survival function, the number of *additional lives* saved thanks to the drone network would vary between 18 and 36 in Virginia Beach over a one-year period of time. This is quite an astonishing result and is most likely an underestimate of the actual number of lives that could be saved with the drone network. Indeed, the above results only take into account the benefits of the drone-based reduced response time for the estimated percentage (15%) of opioid overdoses leading to a cardiac arrest. It is reasonable to assume that the reduced response time will also affect the outcomes of the overdoses not leading to a cardiac arrest. This is corroborated by Ornato et al. who state that: "Every minute that goes by before paramedics or others can attempt resuscitation, an opiate overdose victims' chance of survival decreases by 10 percent" [14, 45].

### 6.2.3 Impact on Quality-adjusted Life Year and Cost Analysis

Quality-adjusted life year (QALY) is a concept commonly used in healthcare economic analyses to evaluate how a healthcare issue impacts a survivor's quality and duration of future life (see, e.g., [9, 51]). A QALY equal to 1 is indicative of one year in perfect health. As shown in (50), the total QALY (T-QALY) for a patient surviving a healthcare problem is the sum of the discounted QALY of each year during one's mean life expectancy after the healthcare incident [9]:

$$T - QALY = \sum_{t=1}^T \frac{\alpha t}{(1+c)^t}, \quad (50)$$

where  $T$  is the number of years of remaining life expectancy,  $\alpha \in [0, 1]$  is a coefficient accounting for the reduced quality of life consecutive to the healthcare incident, and  $c$  is a discount rate reflecting that people prefer good health sooner than later (i.e., a QALY in earlier years is more valuable than in later ones).

To conduct the QALY analysis, we assume, as in [9], that a patient surviving an overdose-associated OHCA has a mean life expectancy of 11.4 years ( $T = 11.4$ ), that each year corresponds to 0.85 QALY ( $\alpha = 0.85$ ), and that the discount rate  $c$  is 3%. Using (50), the T-QALY is equal to 8.47 years for each OHCA survivor (see Table 9 in Appendix D).

Table 6 presents the *additional QALY* gained by using drones instead of ambulances for the survival functions [3], [22], and [18] (see Table 4). The additional QALY attributable to the drone network for the overdose-associated OHCAs in Virginia Beach over one year is very high, varying between 152 and 305 years among the three survival functions.

T-QALY	Survival Function	Number of Survivors		Additional Survivors with Drone Network	Additional QALY in over One Year
		Drone Network	EMS Network		
8.47	Bandara et al. [3]	42	6	36	305
	De Maio et al. [22]	21	3	18	152
	Chanta et al. [18]	35	7	28	237

Table 6: Additional QALY with Drone Network over one Year (from 2018Q3 to 2019Q2)

A drone and the accompanying drone station are estimated to cost \$15,000, to have a four-year lifespan, and to have an annual maintenance cost of \$3,000 [9]. Using these statistics (see Table 10 in Appendix D), the total discounted costs of the eleven drones used in the base scenario amount to \$287,664 (i.e., using a 3% discount rate for the annual maintenance cost) and the drone-based network allows a reduction in the average response time of about 7 minutes and 37 seconds as compared to the ambulance network. That is quite a difference with the option of buying ambulances, each costing between \$150,000 to \$200,000, which, as stated by Burroughs, Ornato et al. [14, 45] would cost “*millions and millions of dollars just to reduce the response time by a minute*” (i.e., from eight to seven).

Assuming that the number of overdoses in Virginia Beach remains stable over four years (i.e., lifespan of a drone), the total additional QALY in four years attributable to the drones network reaches 1220, (resp., 608 and 948) years with the survival function [3] (resp., [22], and [18]), which in turn implies that the proposed drone network only costs \$235 (resp., \$473 and \$303) per incremental QALY. As a benchmark, Bogle et al. report a \$3143 cost per incremental QALY for a network of drones delivering defibrillators to OHCAs in Durham, NC. More generally, it is considered that a medical intervention with a \$50,000 per QALY ratio is cost-effective [42].

Drone Network Cost	Survival Function	Total Additional QALY in Four Years	Cost per Additional QALY
\$287,664	Bandara et al. [3]	1220	\$235
	De Maio et al. [22]	608	\$473
	Chanta et al. [18]	948	\$393

Table 7: Cost Analysis for Drone Network per Incremental QALY ( $p=11$ )

### 6.3 Computational Efficiency

In this section, we conduct a battery of tests to assess the computational efficiency and tractability of the proposed reformulation and algorithms. Section 6.3.1 compares the two proposed algorithmic methods and the direct solution of the reformulated problem with `GUROBI`. Performance profile plots [24] highlight the increased benefits gained with our approaches as the size of the problem and the volume of OTRs increases. Section 6.3.2 assess the sensitivity of the proposed method with respect to the available resources.

All the optimization problems are coded in Python 3.7 and solved with the `GUROBI` 9.1.2 solver on a Linux machine, with Intel Core i7-6700 CPU 3.40GHz processors and 64 GB installed physical memory. For each problem instance, the optimality tolerance is set to 0.01% for each solver, the maximum solution time is set to one hour, and we use one thread only.

#### 6.3.1 Computational Efficiency of Scalability

We evaluate here the computational efficiency and scalability of the proposed reformulation **R-MILP** and algorithms with respect to the size of the problem, more precisely the number  $|I|$  of OTRs to which the network must respond. Using the data described in Section 6.1 and considering the base network scenario with up to 10 DBs and 11 drones, we have created ten problem types that differ in the number of OTRs ranging from 50 to 500, by increment of 50:  $|I| \in \{50, 100, 150, 200, 250, 300, 350, 400, 450, 500\}$ . Each instance type is identified by the tuple  $(q, p, |I|) = (10, 11, |I|)$  and we have generated five problem instances for each instance type. This gives a total of 50 problem instances which we solve with the following approaches:

- **REF0**: Direct solution of problem  $\mathbb{R} - \text{MILP}$  with the default settings of `GUROBI`.
- **OA**: Outer approximation algorithm (Section 5.1).
- **OA-B&C**: Outer Approximation branch-and-cut algorithm (Section 5.2).

The three approaches are compared in terms of solution times and the number of instances for which optimality can be proven in one hour. We note that none of the 50 problem instances formulated with the base formulation **B-IFP** can be solved in one hour with the state-of-the-art solver `BARON` specialized for nonconvex MINLP problems.

We use performance profile plots displayed in (3a) to compare the efficiency of the solution methods. The horizontal axis indicates the running time in seconds while the vertical axis represents the number of instances solved to optimality within the corresponding running time. The solution time for each instance is given in Table 11 in the Appendix.

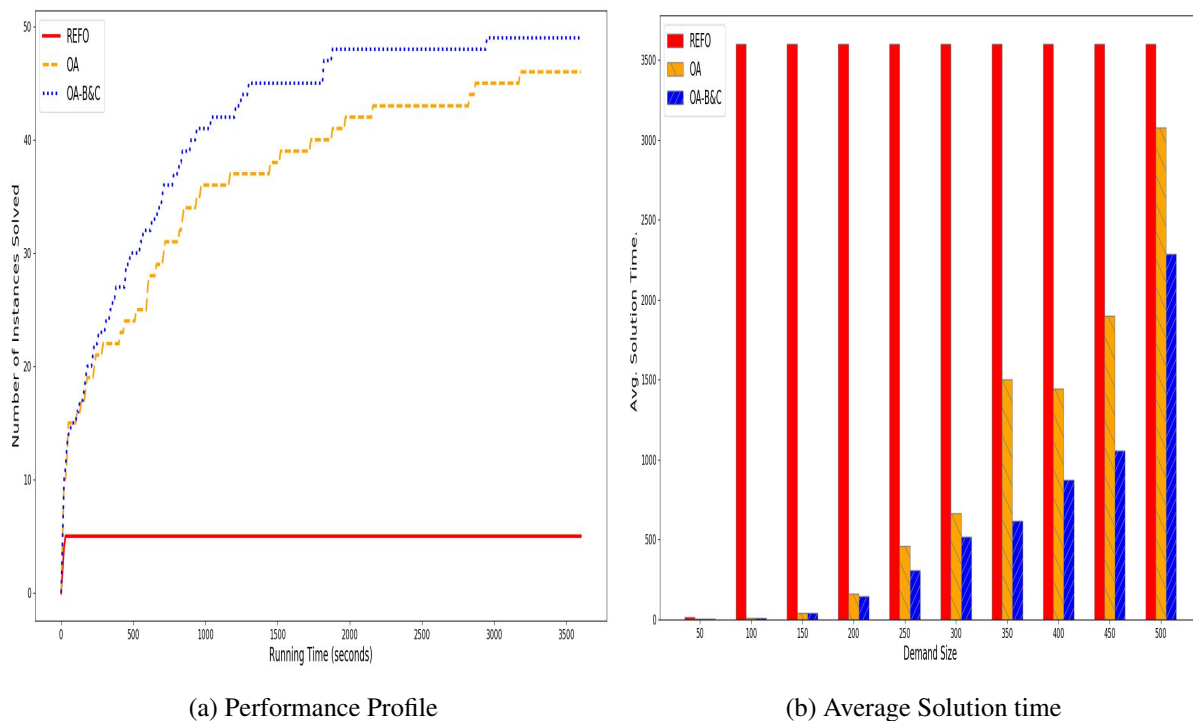


Figure 3: Computational Efficiency for  $(10, 11, |I|)$ : Performance Profile in Figure (3a) and Average Solution Time by Demand Size  $|I|$  in Figure (3b)

The performance profile reveals without any possible ambiguity that the two proposed algorithmic methods OA and OA-B&C are much faster, scale much better, and allow the solution of many more instances than the direct solution method REFO. While the direct solution approach REFO only solves five (i.e. the five smallest instances with  $|I| = 50$  OTRs) of the 50 instances in one hour, OA and OA-B&C solve and prove the optimality of the solution for respectively 46 and 49 instances. Comparing now the algorithms OA and OA-B&C, the dynamic incorporation of valid inequalities and optimality-based cuts permit to further efficiency and scalability gains. This can be seen from the OA-B&C line in the performance plot being above the OA line at any time interval, thereby indicating that the OA-B&C method solves more instances to optimality in any amount of time. As an illustration, Table 12 in Appendix shows that OA-B&C solves 96% of the instances in less than 40 minutes while OA-B needs one hour to solve 92% of the instances.

Figure (3b) shows the average (across five instances) solution times for each instance type and associated size  $|I|$ . When an instance can not be solved to optimality within one hour, the solution time is estimated to be 3600 seconds, which explains that for all instances of size  $|I| \in [100, 500]$  the solution time for REFO is 3600 seconds. Figure (3b) highlights the added benefits of OA-B&C over OA for larger instances. While OA-B&C (blue bar) and OA (orange bar) perform similarly for  $|I| \in [50, 300]$ , OA-B&C solve the instances of larger size  $|I| \in [350, 500]$  much faster than OA can do. For example, OA takes on average about 80% more time than OA-B&C to solve the 450-sized instances.

### 6.3.2 Sensitivity Analysis with Respect to Network Resources

In this section, we evaluate the sensitivity of the solution times with respect to the available network resources and, in particular the number of DBs ( $q$ ) and drones ( $p$ ). We use the algorithm OA-B&C since it enjoys the quickest solution time as shown in Section 6.3.1.

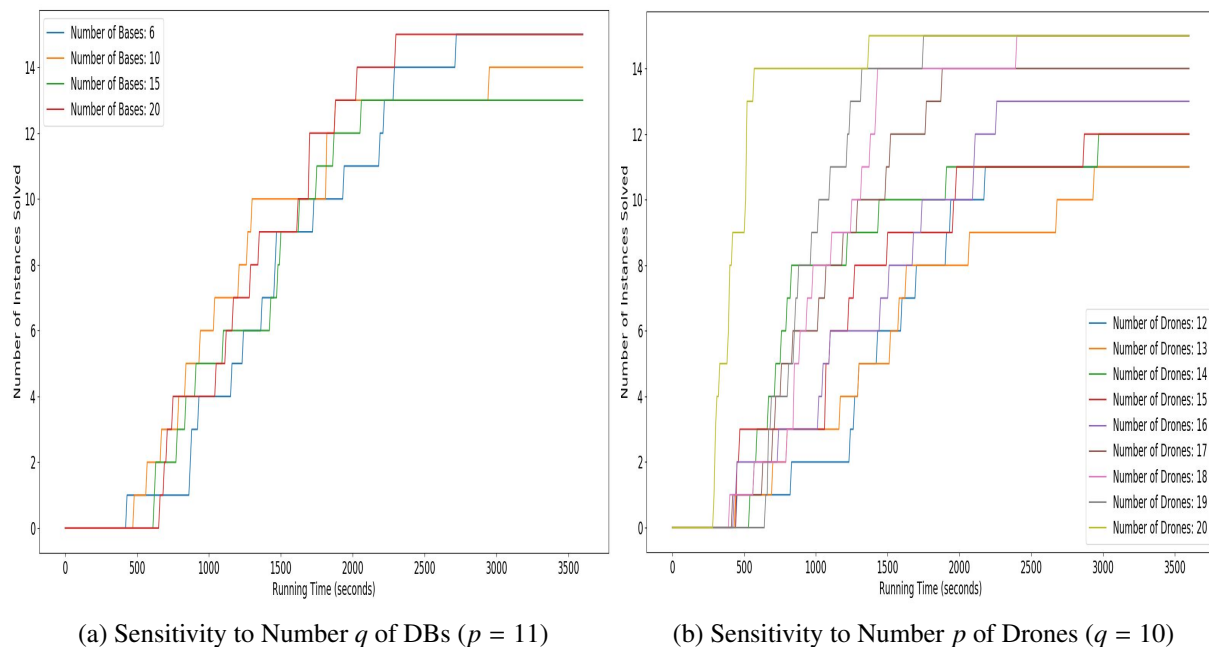


Figure 4: Sensitivity with respect to Number of DBs (Figure (4a)) and Number of Drones (Figure (4b))

We consider four possible values  $q \in \{6, 10, 15, 20\}$  for the number of DBs and three values  $|I| \in \{400, 450, 500\}$  for the demand size (number of OTRs), and generate for each combination of  $q$  and  $|I|$  five problem instances. We assume that  $p = 11$  drones are available. This gives 12 instance types  $(q, 11, |I|)$  for a total of 60 problem instances and we solve each of these with the OA-B&C algorithm. Figure (4a) shows the performance profile associated to each considered number  $q$  of DBs. It appears that the computational time of the OA-B&C method is not particularly sensitive to the number of open DBs since the performance profiles for the considered values of  $q$  intersect, thereby indicating the solution time is not systematically higher (or lower) for any considered number of DBs.

We proceed similarly to evaluate the sensitivity of the computational time with respect to the number of drones. We assume that the maximum number of DBs that can be open is  $q = 10$ . We consider nine possible number of available drones  $p \in \{12, 13, 14, 15, 16, 17, 18, 19, 20\}$ , three possible demand sizes  $|I| \in \{400, 450, 500\}$ , and generate five instances for each of the 27 instance types of each type  $(10, p, |I|)$  for a total of 135 instances that we solve with the OA-B&C method.

The performance profile corresponding to each considered  $p$  is displayed in Figure 4b. It shows that the computational time tends to be quicker (i.e. more instances solved in a given amount of time) when

the number of available drones is larger. We notice in particular that the average solution time is much lower for  $p = 20$  than for any other (smaller) value assigned to  $p$ . A likely explanation for this is that each DB will automatically house two drones when  $q = 10$ .

## 7 Conclusions

Opioid use disorder affects about 2 million Americans and cost about \$78.5 billion in annual health care expenses [23]. In this context, it has been argued that the drone-based delivery of naloxone has the “*potential to be a transformative innovation due to its easily deployable and flexible nature*” [25]. The efficacy of naloxone depends on how quickly it is administered, which is a priority of the US Food and Drug Administration [45]. Buckland et al. [13] argue that further research is needed to “*to develop a decision support system to aid the 911 dispatchers to efficiently assign the drones in a time-sensitive environment*” such as an opioid overdose.

This study responds to the above pressing needs and proposes a new queueing-optimization model to design an EMS network in which drones deliver naloxone to overdose victims in a timely fashion. The objective is to increase the chance of survival of overdose victims by reducing the time needed to deliver and administer naloxone and is accomplished by determining the location of drones and DBs, the capacity of DBs, and the dispatching of drones to overdose incidents. Some new and distinctive features in the model are its survival objective function, the explicit modeling of congestion and decision-dependent (parameter) uncertainty that affects the performance of the network, and its flexibility as the capacity of DBs is not fixed ex-ante but is instead determined by the model.

Besides modeling, the contributions of this study are threefold. On the reformulation side, we propose a tractable MILP reformulation of the stochastic network design problem, which, in its original form, is an NP-hard fractional nonlinear integer optimization problem. We further demonstrate the generalizability of the reformulation approach and prove that the problem of minimizing the average response time in a network organized as a collection of interdependent  $M/G/K$  queueing systems in which the capacity  $K$  of each system is variable is MILP-representable. On the algorithmic side, we derive two algorithmic methods which are significant upgrades over the direct solution of the MILP reformulations. The outer approximation branch-and cut algorithm proves to be the best performing one, significantly reducing solution times, increasing the number of instances solved, and enabling the solution of problems of larger size than those encountered in our case study based on real-life data. On the EMS practice side, the data-driven tests based on overdose data from Virginia Beach reveal that the use of drones to deliver naloxone in response to overdoses could possibly be a game-changer. Besides showing the out-of-sample robustness and applicability of the proposed approach, the tests indeed reveal that using the drone network: 1) the response time is on average close to seven times smaller (1 min and 26 sec) than the one (9 min and 19 sec) with the ambulance network currently in use in Virginia

Beach; 2) the estimated chance of survival to an overdose is more than 4.6 times larger than the one with the Virginia Beach ambulance network; 3) many more lives (of overdose victims) could be saved as compared to the Virginia Beach ambulance network; 4) the total QALY per patient is 8.47 years amounting to up to 305 additional per year across all overdose victims in Virginia Beach, 5) the cost per additional QALY is very low, varying between \$235 and \$473.

This study showcases the potential of using drones to alleviate the devastating consequences of the opioid overdose crisis and could pave the way for the practical implementation of drone-based EMS systems. While very promising, we must however be aware of a number of obstacles for the widespread use of drones to respond to overdoses or other time-critical medical emergencies. These barriers include, for example, regulation, flying condition and zones, safety, data privacy, operations related to the design and maintenance of a medical drone network [30, 47]. While not the focus of this study, future research will be needed on these hindrances as well as on user perceptions and acceptance.

## References

- [1] R. Aboolian, O. Berman, and Z. Drezner. Location and allocation of service units on a congested network. *IIE Transactions* vol. 40 (2008), 422–433.
- [2] A. Atamtürk and V. Narayanan. Polymatroids and Mean-risk Minimization in Discrete Optimization. *Operations Research Letters* vol. 36 (2008), 618–622.
- [3] D. Bandara, M. Mayorga, and L. McLay. Priority dispatching strategies for EMS systems. *Journal of the Operational Research Society* vol. 65 (2014), 572–587.
- [4] R. Batta and O. Berman. A location model for a facility operating as an M/G/k queue. *Networks* vol. 19 (1989), 717–728.
- [5] J. Bauer, D. Moormann, R. Strametz, and D. Groneberg. Development of Unmanned Aerial Vehicle Networks Delivering Early Defibrillation for Out-of-Hospital Cardiac Arrests in Areas Lacking Timely Access to Emergency Medical Services in Germany: A Comparative Economic Study. *BMJ Open* vol. 11 (2021), 1–7.
- [6] O. Berman and D. Krass. Stochastic Location Models with Congestion. *Location Science*. Ed. by G. Laporte, S. Nickel, and F. da Gama. Springer, 2019, 477–535.
- [7] O. Berman and Z. Drezner. The multiple server location problem. *Journal of the Operational Research Society* vol. 58 (2007), 91–99.
- [8] O. Berman, R. C. Larson, and S. S. Chiu. Optimal server location on a network operating as an M/G/1 queue. *Operations Research* vol. 33 (1985), 746–771.
- [9] B. Bogle, W. Rosamond, K. Snyder, and J. Zègre-Hemsey. The Case for Drone-assisted Emergency Response to Cardiac Arrest: An Optimized Statewide Deployment Approach. *North Carolina Medical Journal* vol. 80 (2019), 204–212.
- [10] J. Borrero, C. Gillen, and O. Prokopyev. A Simple Technique to Improve Linearized Reformulations of Fractional (hyperbolic) 0-1 Programming Problems. *Operations Research Letters* vol. 44 (2016), 479–486.

- [11] J. J. Boutilier, S. C. Brooks, A. Janmohamed, A. Byers, J. E. Buick, C. Zhan, A. P. Schoellig, S. Cheskes, L. J. Morrison, and T. C. Chan. Optimizing a drone network to deliver automated external defibrillators. *Circulation* vol. 135 (2017), 2454–2465.
- [12] A. Brill and B. Ganz. The Geographic Variation in the Cost of the Opioid Crisis. 2018.
- [13] D. Buckland, M. Cummings, D. Mark, A. Banerjee, K. Snyder, and M. Starks. Design Considerations for UAV-Delivered Opioid Overdose Interventions. *2019 IEEE Aerospace Conference*. 2019, 1–7.
- [14] D. Burroughs. *It's a bird! It's a plane! It's a drone delivering an overdose-rescue drug?* <https://vadogwood.com/2019/07/22/its-a-bird-its-a-plane-its-a-drone-delivering-an-overdose-rescue-drug/>. [Online; accessed February 5, 2022].
- [15] Centers for Disease Control and Prevention. *Opioid Overdose*. <https://www.cdc.gov/drugoverdose/opioids/index.html>. [Online; accessed February 19, 2022].
- [16] Centers for Disease Control and Prevention. *Overdose Deaths Accelerating During COVID-19*. <https://www.cdc.gov/media/releases/2020/p1218-overdose-deaths-covid-19.html>. [Online; accessed August 19, 2021].
- [17] Centers for Disease Control and Prevention. *Understanding the Epidemic*. <https://www.cdc.gov/opioids/basics/epidemic.html>. [Online; accessed August 19, 2021].
- [18] S. Chanta, M. Mayorga, and L. McLay. The minimum p-envy location problem with requirement on minimum survival rate. *Computers and Industrial Engineering* vol. 74 (2014), 228–239.
- [19] D. Chauhan, A. Unnikrishnan, and M. Figliozzi. Maximum coverage capacitated facility location problem with range constrained drones. *Transportation Research Part C: Emerging Technologies* vol. 99 (2019), 1–18.
- [20] S. S. Chiu and R. C. Larson. Locating an n-server facility in a stochastic environment. *Computers & Operations Research* vol. 12 (1985), 509–516.
- [21] J. Custodio and M. Lejeune. *Spatiotemporal Data Set for Out-of-Hospital Cardiac Arrests*. INFORMS Journal on Computing: Accepted. (2022).
- [22] V. De Maio, I. Stiell, G. Wells, D. Spaite, and G. OPALSS. Optimal Defibrillation Response Intervals for Maximum Out-of-Hospital Cardiac Arrest Survival Rates. *Annals of Emergency Medicine* vol. 42 (2 2003), 242–250.
- [23] C. Dezfulian, A. Orkin, B. Maron, J. Elmer, S. Girotra, M. Gladwin, R. Merchant, A. Panchal, S. Perman, and M. Starks. Opioid-Associated Out-of-Hospital Cardiac Arrest: Distinctive Clinical Features and Implications for Health Care and Public Responses: A Scientific Statement From the American Heart Association. *Circulation* vol. 143 (2021), e836–e870.
- [24] E. Dolan and J. Moré. Benchmarking Optimization Software with Performance Profiles. *Mathematical Programming* vol. 91 (2002), 201–213.
- [25] X. Gao, N. Kong, and P. Griffin. Dynamic optimization of drone dispatch for substance overdose rescue. *2020 Winter Simulation Conference (WSC)*. IEEE. 2020, 830–841.
- [26] J. Góez and M. Anjos. Second-order cone optimization formulations for service system design problems with congestion. *Modeling and Optimization: Theory and Applications*. Ed. by J. Pinter and T. Terlaky. Springer, 2017, 97–120.
- [27] S. L. Hakimi. Optimum Locations of Switching Centers and the Absolute Centers and Medians of a Graph. *Operations Research* vol. 12 (1964), 450–459.

- [28] A. Hart, P. Chai, M. Griswold, J. Lai, E. Boyer, and J. Broach. Acceptability and Perceived Utility of Drone Technology among Emergency Medical Service Responders and Incident Commanders for Mass Casualty Incident Management. *American Journal of Disaster Medicine* vol. 12 (2017), 261–265.
- [29] L. Hellemo, P. Barton, and A. Tomasgard. Decision-dependent probabilities in stochastic programs with recourse. *Computational Management Science* (15 2018), 369–395.
- [30] A. Johnson, C. Cunningham, E. Arnold, W. Rosamond, and J. Zégre-Hemsey. Impact of Using Drones in Emergency Medicine: What Does the Future Hold? *Open Access Emergency Medicine* vol. 2021:13 (2021), 487–498.
- [31] T. Kerensky and A. Walley. Opioid overdose prevention and naloxone rescue kits: what we know and what we don't know. *Addiction Science & Clinical Practice* vol. 12 (2017).
- [32] T. Kleinert, V. Grimm, and M. Schmidt. Outer approximation for global optimization of mixed-integer quadratic bilevel problems. *Mathematical Programming* (2021), 1–61.
- [33] M. Lejeune and F. Margot. *Drone Response to Out-of-Hospital Cardiac Arrests*. Working Paper. 2022.
- [34] H.-L. Li. A Global Approach for General 0–1 Fractional Programming. *European Journal of Operational Research* vol. 73 (1994), 590–596.
- [35] A. Lundell and J. Kronqvist. Integration of polyhedral outer approximation algorithms with MIP solvers through callbacks and lazy constraints. *AIP Conference Proceedings*. Vol. 2070. AIP Publishing LLC. 2019, 020012.
- [36] R. Lynn and J. Galinkin. Naloxone dosage for opioid reversal: current evidence and clinical implications. *Therapeutic Advances in Drug Safety* vol. 9 (2017), 204209861774416.
- [37] V. Marianov and C. ReVelle. The Queueing Maximal availability location problem: A model for the siting of emergency vehicles. *European Journal of Operational Research* vol. 93 (1996), 110–120.
- [38] V. Marianov and C. Revelle. The queuing probabilistic location set covering problem and some extensions. *Socio-Economic Planning Sciences* vol. 28 (1994), 167–178.
- [39] J. Medhi. *Stochastic models in queueing theory*. Elsevier, 2002.
- [40] E. Mehmanchi, A. Gómez, and O. A. Prokopyev. Fractional 0–1 programs: links between mixed-integer linear and conic quadratic formulations. *Journal of Global Optimization* vol. 75 (2019), 273–339.
- [41] M. Moshref-Javadi and M. Winkenbach. Applications and Research Avenues for Drone-based Models in Logistics: A Classification and Review. *Expert Systems with Applications* vol. 177 (2021), 114854.
- [42] P. Neumann, J. Cohen, and M. Weinstein. Updating Cost-Effectiveness— The Curious Resilience of the \$50,000-per-QALY Threshold. *New England Journal of Medicine* vol. 371 (2014), 796–797.
- [43] V. Nimilan, G. Manohar, R. Sudha, and S. Pearley. Drone-aid: An Aerial Medical Assistance. *International Journal of Innovative Technology and Exploring Engineering* vol. 8 (2019), 1288–1292.
- [44] S. A. Nozaki and S. M. Ross. Approximations in finite-capacity multi-server queues by Poisson arrivals. *Journal of Applied Probability* vol. 15 (1978), 826–834.

- [45] J. Ornato, A. You, G. McDiarmid, L. Keyser-Marcus, A. Surrey, J. Humble, S. Dukkipati, L. Harkrader, S. Davis, J. Moyer, D. Tidwell, and A. Mary. Feasibility of bystander-administered naloxone delivered by drone to opioid overdose victims. *The American Journal of Emergency Medicine* vol. 38 (2020), 1787–1791.
- [46] O. Prokopyev, H.-X. Huang, and P. Pardalos. On Complexity of Unconstrained Hyperbolic 0-1 Programming Problems. *Operations Research Letters* vol. 33 (2005), 312–318.
- [47] N. Pulsiri and R. Vatananan-Thesenvitz. Drones in emergency medical services: A Systematic literature review with bibliometric analysis. *International Journal of Innovation and Technology Management* vol. 18 (2021), 2097001.
- [48] N. Pulsiri, R. Vatananan-Thesenvitz, T. Sirisamutr, and P. Wachiradilok. Save Lives: A review of ambulance technologies in pre-hospital emergency medical services. *PICMET 2019 - Portland International Conference on Management of Engineering and Technology: Technology Management in the World of Intelligent Systems* (2019), 1419–1428.
- [49] A. Pulver and R. Wei. Optimizing the spatial location of medical drones. *Applied Geography* vol. 90 (2018), 9–16.
- [50] S. Ross. Chapter 8 - Queueing Theory. *Introduction to Probability Models (Eleventh Edition)*. Ed. by S. Ross. Eleventh Edition. Boston: Academic Press, 2014, 481–558.
- [51] F. Sassi. Calculating QALYs, Comparing QALY and DALY Calculations. *Health Policy Plan* vol. 21 (2006), 402–408.
- [52] A. Sen, A. Atamturk, and P. Kaminsky. A conic integer optimization approach to the constrained assortment problem under the mixed multinomial logit model. *Operations Research* vol. 66 (2018), 994–1003.
- [53] S. Slavova, P. Rock, H. Bush, D. Quesinberry, and S. Walsh. Signal of increased opioid overdose during COVID-19 from emergency medical services data. *Drug Alcohol Depend* vol. 214 (2020), 108176.
- [54] Society of Actuaries. *Economic Impact of Non-Medical Opioid Use in the United States*. <https://www.soa.org/globalassets/assets/files/resources/research-report/2019/econ-impact-non-medical-opioid-use.pdf>. [Online; accessed August 19, 2021].
- [55] C. Tukul, M. Tukul, R. Weinbaum, V. Mika, and P. Levy. Time-to-scene for opioid overdoses: are unmanned aerial drones faster than traditional first responders in an urban environment? *BMJ Innovations* vol. 6 (2020), 204–208.
- [56] P. Van de Voorde, S. Gautama, A. Momont, C.-M. Ionescu, P. De Paepe, and N. Fraeyman. The drone ambulance [A-UAS]: Golden bullet or just a blank? *Resuscitation* vol. 116 (2017), 46–48.
- [57] World Health Organization. *Opioid Overdose*. <https://www.who.int/news-room/fact-sheets/detail/opioid-overdose>. [Online; accessed August 19, 2021]. 2020.
- [58] J. Ye, C. Zhang, J. R. Nickenig Vissoci, and D. Buckland. Optimizing a Drone Network to Deliver Naloxone. *Annals of Emergency Medicine* vol. 74 (2019), S64.

## Appendix A Notations

### A.1 Sets and Indices

$i \in I$ : Index and set of OTR locations.

$j \in J$ : Index and set of candidate DBs.

$i \in I_j$ : Index and set of OTRs that are within the catchment area of a drone at DB  $j$ .

$j \in J_i$ : Index and set of DBs that can cover OTR  $i$ .

### A.2 Parameters and Constants

$A_j$ : Vector of parameters  $(a_j, b_j, c_j)$  representing the coordinates of DB  $j$  in the earth-centered, earth-fixed coordinate system.

$A_i$ : Vector of parameters  $(a_i, b_i, c_i)$  representing the location of OTR  $i$  in the earth-centered, earth-fixed coordinate system.

$M$ : Maximum number of drones that can be stationed at any DB.

$d_{ij}$ : Distance between OTR  $i$  and candidate DB  $j$ .

$v$ : Flight speed of drones.

$\lambda_i$ : OTR arrival rate from location  $i$ .

$p$ : Maximal number of available drones.

$q$ : Maximal number of drone bases that can be established.

$\beta$ : Coefficient modulating the travel speed to and from an OTR location.

$r$ : flight radius of a drone.

### A.3 Decision Variables

$x_j$ : Binary variable determining if a DB is open at candidate location  $j$  ( $x_j = 1$ ) or not ( $x_j = 0$ ).

$y_{ij}$ : Binary variable defining if OTR at location  $i$  is assigned to open DB  $j$  ( $y_{ij} = 1$ ) or not ( $y_{ij} = 0$ ).

$\gamma_j^m$ : Binary integer variable indicating the number  $m$  of drones deployed at DB  $j$ :  $\gamma_j^1 = 1$  if and only one drone is positioned at DB  $j$  and  $\gamma_j^2 = 1$  if and only two drones are positioned at DB  $j$ .

$K_j$ : General integer variable defining the number of drones stationed at DB  $j$ .

$\eta_j$ : Arrival rate of OTRs serviced by DB  $j$ .

$U_j^m$ : Auxiliary variable set equal to the fractional terms in (26) and (27), respectively.

$\mu_{ij}^m$ : Auxiliary variable introduced to linearize bilinear terms  $U_j^m y_{ij}$ .

$z_{it}^j$ : Auxiliary variable introduced to linearize bilinear terms  $y_{ij} y_{lj}$ .

$\tau_{it}^j$ : Auxiliary variable introduced to linearize bilinear terms  $U_j^2 z_{it}^j$ .

$\omega_{ij}^m$ : Auxiliary variable introduced to linearize bilinear terms  $\gamma_j^m \mu_{ij}^m$ .

#### A.4 Random Variables

$S_{ij}$ : Service time for OTR at  $i$  if serviced with a drone stationed at DB  $j$ .

$S_j$ : Service time of a drone at DB  $j$ .

$Q_j$ : Queueing delay time for DB  $j$ .

$R_i$ : Response time between reception of the delivery request and arrival of a drone for an OTR at  $i$ .

$\alpha_i$ : On-scene service time (e.g. naloxone toolkit unloading time) for location  $i$ .

$\epsilon_i$ : Drone reset time needed to recharge and load new naloxone toolkit for location  $i$ .

$\xi_i$ : Non-travel drone service time equal to  $\alpha_i + \epsilon_i$  for OTR at location  $i$ .

## Appendix B Drone-delivery Network for Opioid Overdoses- Illustration

We use a small network to illustrate the formulations presented in this study. We consider two candidate locations for drone bases (DB  $j=1$  and  $j=2$ ) which can each house at most two ( $M$ ) drones. There are three OTRs ( $i = 1, 2, 3$ ). Requests  $i = 1$  and  $i = 2$  are within the catchment area of a drone positioned at DB  $j = 1$  while requests  $i = 2$  and  $i = 3$  are within the catchment area of a drone at DB  $j = 2$ . Figure 5 provides a visualization of the network. The solid circle represents DBs while the dotted circles represent catchment areas of a DB and its drones. The diamonds are the locations of the overdose incidents.

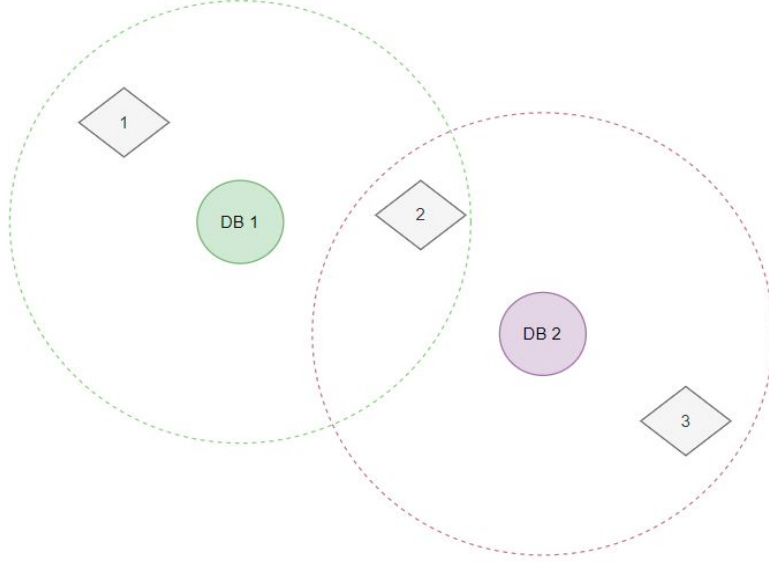


Figure 5: Small Drone Network and OTRs

The objective function (11a) of problem **B-IFP** can be written as:

$$\begin{aligned}
 \min \frac{1}{\lambda_1 + \lambda_2 + \lambda_3} & \left[ \frac{\lambda_1 d_{11} y_{11}}{v} + \frac{\lambda_2 d_{21} y_{21}}{v} + \frac{\lambda_2 d_{22} y_{22}}{v} + \frac{\lambda_3 d_{32} y_{32}}{v} + \right. \\
 & \frac{\lambda_1 y_{11} (\lambda_1 y_{11} \mathbb{E}[S_{11}^2] + \lambda_2 y_{21} \mathbb{E}[S_{21}^2]) (\lambda_1 y_{11} \mathbb{E}[S_{11}] + \lambda_2 y_{21} \mathbb{E}[S_{21}])}{2(2 - (\lambda_1 y_{11} \mathbb{E}[S_{11}] + \lambda_2 y_{21} \mathbb{E}[S_{21}]))^2 [1 + (\lambda_1 y_{11} \mathbb{E}[S_{11}] + \lambda_2 y_{21} \mathbb{E}[S_{21}]) + \frac{(\lambda_1 y_{11} \mathbb{E}[S_{11}] + \lambda_2 y_{21} \mathbb{E}[S_{21}])^2}{2 - (\lambda_1 y_{11} \mathbb{E}[S_{11}] + \lambda_2 y_{21} \mathbb{E}[S_{21}])}]} \\
 & \frac{\lambda_2 y_{21} (\lambda_1 y_{11} \mathbb{E}[S_{11}^2] + \lambda_2 y_{21} \mathbb{E}[S_{21}^2]) (\lambda_1 y_{11} \mathbb{E}[S_{11}] + \lambda_2 y_{21} \mathbb{E}[S_{21}])}{2(2 - (\lambda_1 y_{11} \mathbb{E}[S_{11}] + \lambda_2 y_{21} \mathbb{E}[S_{21}]))^2 [1 + (\lambda_1 y_{11} \mathbb{E}[S_{11}] + \lambda_2 y_{21} \mathbb{E}[S_{21}]) + \frac{(\lambda_1 y_{11} \mathbb{E}[S_{11}] + \lambda_2 y_{21} \mathbb{E}[S_{21}])^2}{2 - (\lambda_1 y_{11} \mathbb{E}[S_{11}] + \lambda_2 y_{21} \mathbb{E}[S_{21}])}]} \\
 & \frac{\lambda_2 y_{22} (\lambda_2 y_{22} \mathbb{E}[S_{22}^2] + \lambda_3 y_{32} \mathbb{E}[S_{32}^2]) (\lambda_2 y_{22} \mathbb{E}[S_{22}] + \lambda_3 y_{32} \mathbb{E}[S_{32}])}{2(2 - (\lambda_2 y_{22} \mathbb{E}[S_{22}] + \lambda_3 y_{32} \mathbb{E}[S_{32}]))^2 [1 + (\lambda_2 y_{22} \mathbb{E}[S_{22}] + \lambda_3 y_{32} \mathbb{E}[S_{32}]) + \frac{(\lambda_2 y_{22} \mathbb{E}[S_{22}] + \lambda_3 y_{32} \mathbb{E}[S_{32}])^2}{2 - (\lambda_2 y_{22} \mathbb{E}[S_{22}] + \lambda_3 y_{32} \mathbb{E}[S_{32}])}]} \\
 & \left. \frac{\lambda_3 y_{32} (\lambda_2 y_{22} \mathbb{E}[S_{22}^2] + \lambda_3 y_{32} \mathbb{E}[S_{32}^2]) (\lambda_2 y_{22} \mathbb{E}[S_{22}] + \lambda_3 y_{32} \mathbb{E}[S_{32}])}{2(2 - (\lambda_2 y_{22} \mathbb{E}[S_{22}] + \lambda_3 y_{32} \mathbb{E}[S_{32}]))^2 [1 + (\lambda_2 y_{22} \mathbb{E}[S_{22}] + \lambda_3 y_{32} \mathbb{E}[S_{32}]) + \frac{(\lambda_2 y_{22} \mathbb{E}[S_{22}] + \lambda_3 y_{32} \mathbb{E}[S_{32}])^2}{2 - (\lambda_2 y_{22} \mathbb{E}[S_{22}] + \lambda_3 y_{32} \mathbb{E}[S_{32}])}]} \right]
 \end{aligned}$$

The objective function (12a) of problem **R-BFP** can be written as:

$$\begin{aligned}
\min \frac{1}{\lambda_1 + \lambda_2 + \lambda_3} & \left[ \frac{\lambda_1 d_{11} y_{11}}{v} + \frac{\lambda_2 d_{21} y_{21}}{v} + \frac{\lambda_2 d_{22} y_{22}}{v} + \frac{\lambda_3 d_{32} y_{32}}{v} + \right. \\
& \frac{\lambda_1 y_{11} \gamma_1^1 (\lambda_1 y_{11} \mathbb{E}[S_{11}^2] + \lambda_2 y_{21} \mathbb{E}[S_{21}^2])}{2(1 - (\lambda_1 y_{11} \mathbb{E}[S_{11}] + \lambda_2 y_{21} \mathbb{E}[S_{21}]))^2 \left[ 1 + \frac{\lambda_1 y_{11} \mathbb{E}[S_{11}] + \lambda_2 y_{21} \mathbb{E}[S_{21}]}{1 - (\lambda_1 y_{11} \mathbb{E}[S_{11}] + \lambda_2 y_{21} \mathbb{E}[S_{21}])} \right]} + \\
& \frac{\lambda_1 y_{11} \gamma_1^2 (\lambda_1 y_{11} \mathbb{E}[S_{11}^2] + \lambda_2 y_{21} \mathbb{E}[S_{21}^2]) (\lambda_1 y_{11} \mathbb{E}[S_{11}] + \lambda_2 y_{21} \mathbb{E}[S_{21}])}{2(2 - (\lambda_1 y_{11} \mathbb{E}[S_{11}] + \lambda_2 y_{21} \mathbb{E}[S_{21}]))^2 \left[ 1 + (\lambda_1 y_{11} \mathbb{E}[S_{11}] + \lambda_2 y_{21} \mathbb{E}[S_{21}]) + \frac{(\lambda_1 y_{11} \mathbb{E}[S_{11}] + \lambda_2 y_{21} \mathbb{E}[S_{21}])^2}{2 - (\lambda_1 y_{11} \mathbb{E}[S_{11}] + \lambda_2 y_{21} \mathbb{E}[S_{21}])} \right]} + \\
& \frac{\lambda_2 y_{21} \gamma_1^1 (\lambda_1 y_{11} \mathbb{E}[S_{11}^2] + \lambda_2 y_{21} \mathbb{E}[S_{21}^2])}{2(1 - (\lambda_1 y_{11} \mathbb{E}[S_{11}] + \lambda_2 y_{21} \mathbb{E}[S_{21}]))^2 \left[ 1 + \frac{(\lambda_1 y_{11} \mathbb{E}[S_{11}] + \lambda_2 y_{21} \mathbb{E}[S_{21}])}{1 - (\lambda_1 y_{11} \mathbb{E}[S_{11}] + \lambda_2 y_{21} \mathbb{E}[S_{21}])} \right]} + \\
& \frac{\lambda_2 y_{21} \gamma_1^2 (\lambda_1 y_{11} \mathbb{E}[S_{11}^2] + \lambda_2 y_{21} \mathbb{E}[S_{21}^2]) (\lambda_1 y_{11} \mathbb{E}[S_{11}] + \lambda_2 y_{21} \mathbb{E}[S_{21}])}{2(2 - (\lambda_1 y_{11} \mathbb{E}[S_{11}] + \lambda_2 y_{21} \mathbb{E}[S_{21}]))^2 \left[ 1 + (\lambda_1 y_{11} \mathbb{E}[S_{11}] + \lambda_2 y_{21} \mathbb{E}[S_{21}]) + \frac{(\lambda_1 y_{11} \mathbb{E}[S_{11}] + \lambda_2 y_{21} \mathbb{E}[S_{21}])^2}{2 - (\lambda_1 y_{11} \mathbb{E}[S_{11}] + \lambda_2 y_{21} \mathbb{E}[S_{21}])} \right]} + \\
& \frac{\lambda_2 y_{22} \gamma_2^1 (\lambda_2 y_{22} \mathbb{E}[S_{22}^2] + \lambda_3 y_{32} \mathbb{E}[S_{32}^2])}{2(1 - (\lambda_2 y_{22} \mathbb{E}[S_{22}] + \lambda_3 y_{32} \mathbb{E}[S_{32}]))^2 \left[ 1 + \frac{\lambda_2 y_{22} \mathbb{E}[S_{22}] + \lambda_3 y_{32} \mathbb{E}[S_{32}]}{1 - (\lambda_2 y_{22} \mathbb{E}[S_{22}] + \lambda_3 y_{32} \mathbb{E}[S_{32}])} \right]} + \\
& \frac{\lambda_2 y_{22} \gamma_2^2 (\lambda_2 y_{22} \mathbb{E}[S_{22}^2] + \lambda_3 y_{32} \mathbb{E}[S_{32}^2]) (\lambda_2 y_{22} \mathbb{E}[S_{22}] + \lambda_3 y_{32} \mathbb{E}[S_{32}])}{2(2 - (\lambda_2 y_{22} \mathbb{E}[S_{22}] + \lambda_3 y_{32} \mathbb{E}[S_{32}]))^2 \left[ 1 + (\lambda_2 y_{22} \mathbb{E}[S_{22}] + \lambda_3 y_{32} \mathbb{E}[S_{32}]) + \frac{(\lambda_2 y_{22} \mathbb{E}[S_{22}] + \lambda_3 y_{32} \mathbb{E}[S_{32}])^2}{2 - (\lambda_2 y_{22} \mathbb{E}[S_{22}] + \lambda_3 y_{32} \mathbb{E}[S_{32}])} \right]} + \\
& \frac{\lambda_3 y_{32} \gamma_2^1 (\lambda_2 y_{22} \mathbb{E}[S_{22}^2] + \lambda_3 y_{32} \mathbb{E}[S_{32}^2])}{2(1 - (\lambda_2 y_{22} \mathbb{E}[S_{22}] + \lambda_3 y_{32} \mathbb{E}[S_{32}]))^2 \left[ 1 + \frac{\lambda_2 y_{22} \mathbb{E}[S_{22}] + \lambda_3 y_{32} \mathbb{E}[S_{32}]}{1 - (\lambda_2 y_{22} \mathbb{E}[S_{22}] + \lambda_3 y_{32} \mathbb{E}[S_{32}])} \right]} + \\
& \left. \frac{\lambda_3 y_{32} \gamma_2^2 (\lambda_2 y_{22} \mathbb{E}[S_{22}^2] + \lambda_3 y_{32} \mathbb{E}[S_{32}^2]) (\lambda_2 y_{22} \mathbb{E}[S_{22}] + \lambda_3 y_{32} \mathbb{E}[S_{32}])}{2(2 - (\lambda_2 y_{22} \mathbb{E}[S_{22}] + \lambda_3 y_{32} \mathbb{E}[S_{32}]))^2 \left[ 1 + (\lambda_2 y_{22} \mathbb{E}[S_{22}] + \lambda_3 y_{32} \mathbb{E}[S_{32}]) + \frac{(\lambda_2 y_{22} \mathbb{E}[S_{22}] + \lambda_3 y_{32} \mathbb{E}[S_{32}])^2}{2 - (\lambda_2 y_{22} \mathbb{E}[S_{22}] + \lambda_3 y_{32} \mathbb{E}[S_{32}])} \right]} \right]
\end{aligned}$$

The objective function (24a) of problem **R-MILP** can be written as:

$$\begin{aligned}
\min \frac{1}{\lambda_1 + \lambda_2 + \lambda_3} & \left[ \frac{\lambda_1 d_{11} y_{11}}{v} + \frac{\lambda_2 d_{21} y_{21}}{v} + \frac{\lambda_2 d_{22} y_{22}}{v} + \frac{\lambda_3 d_{32} y_{32}}{v} + \right. \\
& \left. \lambda_1 \left( \frac{\omega_{11}^1}{2} + \frac{\omega_{11}^2}{2} \right) + \lambda_2 \left( \frac{\omega_{21}^1}{2} + \frac{\omega_{21}^2}{2} + \frac{\omega_{22}^1}{2} + \frac{\omega_{22}^2}{2} \right) + \lambda_3 \left( \frac{\omega_{32}^1}{2} + \frac{\omega_{32}^2}{2} \right) \right]
\end{aligned}$$

## Appendix C Size of Formulations

	<b>B – IFP</b>	<b>R – BFP</b>
Number of constraints	$\sum_{i \in I}  J_i  +  I  + 2 J  + 2$	$\sum_{i \in I}  J_i  +  I  + 3 J  + 2$
Number of binary variables	$\sum_{i \in I}  J_i  +  J $	$\sum_{i \in I}  J_i  + (M + 1) J $
Number of general integer variables	$ J $	0

Table 8: Dimensions of Problems **B – IFP** and **R – BFP**

## Appendix D Data for QALY and Cost Analysis

$T$	$\alpha$	$c$	T-QALY
11.4 years	0.85	3%	8.47 years

Table 9: QALY Analysis for each OHCA Survivor

Price per Drone	Annual Maintenance Cost	Number of Drones	Discount Rate	Total Discounted Cost in 4 Years.
\$15,000	\$3,000	11	3%	\$287,664

Table 10: Cost for Drone Network

## Appendix E Computational Efficiency Study

I	Instance	Solution Time (sec.)		
		REFO	OA	OA-B&C
50	1	7	3	3
	2	25	3	3
	3	17	2	2
	4	17	3	3
	5	6	3	2
	Average	14	3	3
100	1	3600	12	11
	2	3600	13	12
	3	3600	11	10
	4	3600	12	12
	5	3600	12	12
	Average	3600	12	11
150	1	3600	46	60
	2	3600	47	33
	3	3600	37	29
	4	3600	41	43
	5	3600	39	32
	Average	3600	42	39
200	1	3600	170	151
	2	3600	109	105
	3	3600	161	122
	4	3600	138	170
	5	3600	221	169
	Average	3600	160	143
250	1	3600	706	358
	2	3600	517	302
	3	3600	408	227
	4	3600	431	440
	5	3600	233	218
	Average	3600	459	309
300	1	3600	831	252
	2	3600	608	374
	3	3600	935	706
	4	3600	656	813
	5	3600	288	446
	Average	3600	664	518
350	1	3600	595	699
	2	3600	1160	540
	3	3600	3172	893
	4	3600	710	620
	5	3600	1872	337
	Average	3600	1502	618
400	1	3600	1515	778
	2	3600	1442	560
	3	3600	2824	1249
	4	3600	596	1295
	5	3600	847	471
	Average	3600	1445	871
450	1	3600	965	669
	2	3600	2155	934
	3	3600	3600	1815
	4	3600	810	833
	5	3600	1966	1033
	Average	3600	1899	1057
500	1	3600	3600	2943
	2	3600	3600	1814
	3	3600	3600	3600
	4	3600	2865	1208
	5	3600	1728	1872
	Average	3600	3079	2287

Table 11: Computational Efficiency for Base Case Scenario:  $q = 10$  and  $p = 11$

Solution Time (seconds)	REFO	OA	OA-B&C
600	10%	54%	64%
1200	10%	74%	84%
1800	10%	80%	90%
2400	10%	86%	96%
3000	10%	90%	98%
3600	10%	92%	98%

Table 12: Percentage of Problem Instances Solved to Optimality